

# The performance of approximate equation of motion coupled cluster for valence and core states of heavy element systems

Loïc Halbert<sup>1, a)</sup> and André Severo Pereira Gomes<sup>1, b)</sup>

*Université de Lille, CNRS, UMR 8523—PhLAM—Physique des Lasers Atomes et Molécules, F-59000 Lille, France*

(Dated: 6 July 2023)

The equation of motion coupled cluster singles and doubles model (EOM-CCSD) is an accurate, black-box correlated electronic structure approach to investigate electronically excited states and electron attachment or detachment processes. It has also served as a basis for developing less computationally expensive approximate models such as partitioned EOM-CCSD (P-EOM-CCSD), the second-order many-body perturbation theory EOM (EOM-MBPT(2)), and their combination (P-EOM-MBPT(2)) [S. Gwaltney et al., *Chem. Phys. Lett.* **248**, 189-198 (1996)]. In this work we outline an implementation of these approximations for four-component based Hamiltonians and investigate their accuracy relative to EOM-CCSD for valence excitations, valence and core ionizations and electron attachment, and this for a number of systems of atmospheric or astrophysical interest containing elements across the periodic table. We have found that across the different systems and electronic states of different nature considered, partition EOM-CCSD yields results with the largest deviations from the reference, whereas second-order based approaches tend show a generally better agreement with EOM-CCSD. We trace this behavior to the imbalance brought about by the removal of excited state relaxation in the partition approaches, with respect to degree of electron correlation recovered.

## I. INTRODUCTION

Developments in electronic structure methods of recent decades<sup>1-3</sup> have allowed theory to play a more important role in helping interpret increasingly complex experiments. One case arises in connection to the recent developments on coherent light sources such as those generated in synchrotrons<sup>4-7</sup> or X-ray free-electron lasers (XFEL)<sup>8,9</sup>, which have enabled significant improvements in resolution when exploring high-energy processes involving electronic excitations, such as in X-ray absorption spectroscopy (XAS). But theory can also be of help in lower-energy regimes, be in photoionization experiments<sup>10</sup> in UV/visible energy range or in the determination of electron affinities<sup>11-13</sup>.

Among the approaches that are generally capable of treating core and valence excited states, as well states representing electron attachment and detachment processes, we find methods such as complete-active space second-order perturbation theory (CASPT2)<sup>14,15</sup> and multireference CI (MRCI)<sup>16</sup>, which thanks to their flexibility can describe systems which are multiconfigurational already for their ground states. For systems which the ground-state can be well-represented by a single configuration an array of other methods are also available, such as time-dependent DFT (TD-DFT)<sup>17-21</sup>, the algebraic diagrammatic construction (ADC) family of methods<sup>22,23</sup>, as well as the family of methods based on coupled cluster theory, such as linear-response (LR-CC)<sup>24,25</sup> and equation of motion (EOM)<sup>25-32</sup> coupled cluster.

It should be noted that for certain situations such as in the calculation of core and valence ionization energies, methods based on the calculation of energy differences (such  $\Delta\text{HF}$ <sup>33-35</sup>,

$\Delta\text{MP2}$ <sup>36,37</sup>,  $\Delta\text{DFT}$ <sup>20,38-40</sup>,  $\Delta\text{CC}$ <sup>41,42</sup>) can be very useful, since they are very effective in accounting for orbital relaxation (upon ionization) and electron correlation, but at the expense of requiring the solution of the mean-field problem for open-shells that may be difficult to converge, not to mention the need to find broken symmetry solutions when equivalent centers are present.

Thus, when single-reference approaches are applicable, a good balance between ease of use and accuracy for both valence and core processes is found in coupled cluster based approaches such as EOM-CC (or equivalently LR-CC) based on the coupled cluster singles doubles (CCSD) model. That said, in view of the still significant computational cost of CCSD it is interesting to explore to which extent approximations to EOM-CCSD can still provide accurate results while reducing computational cost.

Two main classes of approximations that show promise for valence and core state but that nevertheless have not been extensively explored are partition EOM-CCSD (P-EOM-CCSD<sup>43-46</sup>), which approximates the doubles-doubles block of matrix representation of the similarity transformed Hamiltonian, and a second-order approximation to EOM-CC (EOM-MBPT(2))<sup>47-50</sup> in which, the matrix elements of similarity transformed Hamiltonian are approximated to second order.

To date and to the best of our knowledge, explorations of P-EOM-CCSD and (P-)EOM-MBPT(2) have been carried out for non-relativistic Hamiltonians. However, it is now widely recognized that in order to arrive at qualitative and quantitative agreement with experiment, relativistic effects<sup>51-54</sup> must be taken into account for valence processes of molecules containing elements from the middle to the bottom of the periodic table, and for core processes of molecules containing relatively light elements such as chloride<sup>55</sup>.

The aim of this paper is therefore to extend our work on relativistic EOM-CCSD for valence<sup>56</sup> and core<sup>57</sup> states, in order to present a pilot implementation of P-EOM-CCSD and (P-)EOM-MBPT(2) in the DIRAC code, and assess their per-

<sup>a)</sup>Electronic mail: loic.halbert@univ-lille.fr

<sup>b)</sup>Author to whom correspondence should be addressed; Electronic mail: andre.gomes@univ-lille.fr

formance with respect to EOM-CCSD for benchmark systems containing heavy and superheavy elements—with a particular emphasis on halogenated species, in view of their importance to atmospheric chemistry and physics<sup>58,59</sup>.

This paper is organized as follows : after a brief review of the formalism for P-EOM-CCSD, EOM-MBPT(2) and P-EOM-MBPT(2), we compare their performance to that of EOM-CCSD for (a) valence ionizations of  $I_3^-$  and halogen monoxide ions  $XO^-$  ( $X$ : Cl, Br, I, At); (b) core ionizations of HCl, HBr and  $I^-$ ; (c) electron affinities of  $I_3^-$ ,  $CH_2I_2$  and  $CH_2IBr$ ; and (d) excitation energies of  $I_3^-$  et  $CH_2I_2$ , followed by our conclusions and perspectives for future work.

## II. THEORY

### A. Equation of motion coupled cluster

The Coupled-Cluster wave function  $|\Phi_{CC}\rangle$  is defined as 26 :

$$|\Phi_{CC}\rangle = e^{\hat{T}}|\Phi_0\rangle, \quad (1)$$

where  $|\Phi_0\rangle$  denotes the Hartree-Fock determinant for the ground-state and  $\hat{T}$  the cluster operator, which here shall be restricted to single and double excitations,

$$\hat{T} = \hat{T}_1 + \hat{T}_2 = \sum_{ia} t_i^a \{\hat{a}_a^\dagger \hat{a}_i\} + \frac{1}{4} \sum_{abij} t_{ij}^{ab} \{\hat{a}_a^\dagger \hat{a}_b^\dagger \hat{a}_j \hat{a}_i\} \quad (2)$$

with  $\hat{a}^\dagger$  and  $\hat{a}$  denoting respectively creation and annihilation operators and  $t_i^a$  and  $t_{ij}^{ab}$  the corresponding amplitudes to be determined. Here, and in the following :  $a, b, c, \dots$  will indicate particle lines,  $i, j, k, \dots$  hole lines, and  $p, q, r, s, \dots$  either holes or particles<sup>60</sup>.

In order to defined the EOM-CCSD method, define first the normal-ordered Hamiltonian

$$\begin{aligned} \hat{H}_N &= \hat{H} - \langle \Phi_0 | \hat{H} | \Phi_0 \rangle \\ &= \sum_{pq} \langle p | f | q \rangle \{\hat{a}_p^\dagger \hat{a}_q\} + \frac{1}{4} \sum_{pqrs} \langle pq || rs \rangle \{\hat{a}_p^\dagger \hat{a}_q^\dagger \hat{a}_s \hat{a}_r\} \\ &= \sum_{pq} f_{pq} \{\hat{a}_p^\dagger \hat{a}_q\} + \frac{1}{4} \sum_{pqrs} g_{pqrs} \{\hat{a}_p^\dagger \hat{a}_q^\dagger \hat{a}_s \hat{a}_r\} \end{aligned} \quad (3)$$

where  $f_{pq}$  and  $g_{pqrs}$  represent the matrix/tensor representations of the Fock operator and 2-electrons integral respectively; and second, the similarity transformed Hamiltonian  $\bar{H}$ ,

$$\bar{H} = e^{-\hat{T}} \hat{H}_N e^{\hat{T}}. \quad (4)$$

With these, and choosing a parametrization of electronic states other than the ground state on the basis of a reference coupled cluster wavefunction,

$$|\Phi_x\rangle = \mathcal{R}|\Phi_{CC}\rangle = \mathcal{R}e^{\hat{T}}|\Phi_0\rangle \quad (5)$$

the EOM problem for electronically excited, electron attachment and electron detachment states is given by an eigenvalue equation

$$\bar{H}\mathbf{R} = \omega\mathbf{R}, \quad (6)$$

that is solved by standard iterative procedures (see<sup>56,57</sup> and references therein).

The operator  $\mathcal{R}$ , for excited states (EE) is given by the linear expansion

$$\mathcal{R}^{EE} = r_0 + r_i^a \hat{a}_a^\dagger \hat{a}_i + \frac{1}{4} r_{ij}^{ab} \hat{a}_a^\dagger \hat{a}_b^\dagger \hat{a}_j \hat{a}_i; \quad (7)$$

with  $r_0 = 1$  for the ground-state and  $r_0 = 0$  otherwise; for electron detachment (ionization energies, IP) a particle line disappears, yielding

$$\mathcal{R}^{IP} = r_i \hat{a}_i + \frac{1}{2} r_{ij}^a \hat{a}_a^\dagger \hat{a}_i \hat{a}_j, \quad (8)$$

whereas for electron attachment (electron affinities, EA) a hole line disappears, yielding

$$\mathcal{R}^{EA} = r^a \hat{a}_a^\dagger + \frac{1}{2} r_i^{ab} \hat{a}_a^\dagger \hat{a}_i \hat{a}_b^\dagger, \quad (9)$$

However, in all of these cases we can identify the same block structure in the matrix representation of  $\bar{H}$ ,

$$\begin{pmatrix} \bar{H}_{SS} & \bar{H}_{SD} \\ \bar{H}_{DS} & \bar{H}_{DD} \end{pmatrix} \quad (10)$$

consisting of matrix elements between singly excited (1h1p), attached (1p) or detached (1h) configuration ( $\bar{H}_{SS}$ ); between doubly excited (2h2p), or singly attachment or detachment configurations accompanied by relaxation (2p1h/2h1p) ( $\bar{H}_{DD}$ ); and between these two manifolds ( $\bar{H}_{SD}$  and  $\bar{H}_{DS}$ ).

To obtain the ionization potentials of the core electrons, we use the Core-Valence-Separation (CVS) technique<sup>22,25,61</sup>, in which the eigenvector vector solution  $\mathbf{R}_k$  is limited in size by the fact of taking into account only the molecular orbitals (MO) lower than a certain value in energy arbitrarily defining the valence/core limit. For algorithm we use a projection operator  $\mathcal{P}$  working on the trial vector  $\sigma$ <sup>56</sup> which acts on a molecular orbital  $i$  to a virtual molecular orbital  $a$ , only if  $i$  belongs to the core space (labelled "I").

$$\begin{cases} \mathcal{P}_I \sigma_i^a = 0 & \text{if } i \neq I \\ \mathcal{P}_I \sigma_{ij}^{ab} = 0 & \text{if } i \neq I \text{ or } j \neq I \end{cases} \quad (11)$$

$$\mathcal{P}_I(\mathbf{H}\mathcal{P}_I\mathbf{R}_k) = \omega_k \mathcal{P}_I\mathbf{R}_k \quad (12)$$

This technique had been tested on several system and gives accurate and reproducible results<sup>57</sup>.

### B. Approximated methods

As mentioned before, we shall consider two main families of approximated methods here. The first is the partitioned EOM-CCSD (P-EOM-CCSD). Its starting point is the EOM equation, in which for a given eigenvector  $R_k$  with eigenvalue

$\omega_k$  is separated into two parts; a part of interest 'a' and a part 'b', orthogonal to 'a',

$$\begin{pmatrix} \bar{H}_{SS} & \bar{H}_{SD} \\ \bar{H}_{DS} & \bar{H}_{DD} \end{pmatrix} \begin{pmatrix} R_{k_a} \\ R_{k_b} \end{pmatrix} = \omega_k \begin{pmatrix} R_{k_a} \\ R_{k_b} \end{pmatrix} \quad (13)$$

This expression can be rewritten as

$$\begin{cases} \bar{H}_{SS} \cdot R_{k_a} + \bar{H}_{SD} \cdot R_{k_b} = \omega_k R_{k_a} \\ \bar{H}_{DS} \cdot R_{k_a} + \bar{H}_{DD} \cdot R_{k_b} = \omega_k R_{k_b} \end{cases} \quad (14)$$

and from it one can define an effective Hamiltonian and an associated eigenvalue problem

$$\begin{aligned} \bar{H}_{SS}(\omega_k)_{\text{eff}} &= \bar{H}_{SS} + \bar{H}_{SD}(\omega_k \cdot \mathbb{1} - \bar{H}_{DD})^{-1} \bar{H}_{DS} \\ \bar{H}_{SS}(\omega_k)_{\text{eff}} &= \omega_k R_{k_a} \end{aligned} \quad (15)$$

Carrying out a development limited to the zeroth order<sup>62-64</sup>  $\bar{H}_{DD}$  is replaced by zero-order approximation  $H_{DD}^{[0]}$ , which is diagonal for (semi-)canonical Hartree-Fock orbitals<sup>49</sup>. With that, the EOM-CCSD matrix now becomes

$$\begin{pmatrix} \bar{H}_{SS} & \bar{H}_{SD} \\ \bar{H}_{DS} & \bar{H}_{DD}^{[0]} \end{pmatrix} \quad (16)$$

This method has the advantage of being in  $N^5$ , also for EOM-EE and EOM-EA. Working equations for  $\sigma$ -vectors and intermediates are given in appendix A.

In the EOM-MBPT(2) method<sup>48</sup>, we devising a second-order approximation to the molecular Hamiltonian,

$$\bar{H}^{[2]} = \langle 0 | \bar{H}^{[2]} | 0 \rangle + \mathcal{F}_q^{p[2]} \{ \hat{a}_p^\dagger \hat{a}_q \} + \frac{1}{4} \mathcal{W}_{rs}^{pq[2]} \{ \hat{a}_p^\dagger \hat{a}_q^\dagger \hat{a}_s \hat{a}_r \} + \dots \quad (17)$$

The first term is just the energy of the reference state at the second order perturbation.  $\mathcal{F}_q^{p[2]}$  and  $\mathcal{W}_{rs}^{pq[2]}$  are matrix element, some Effective Hamiltonians, but in fact intermediates (see 65), developed at the second order.

As an example,  $\mathcal{F}_v^v$  depends on  $\tau_{mn}^{ae} = t_{mn}^{ae} + t_m^a t_n^e - t_m^e t_n^a$ , but now :

$$\begin{aligned} \mathcal{F}_v^v &= \mathcal{F}_b^a = f_b^a - t_m^a f_b^m + t_m^f \langle ma || fb \rangle \\ &- \frac{1}{2} \left\{ \begin{array}{l} \text{Complete : } \tau_{mn}^{ae} \langle mn || be \rangle \\ \text{MBPT(2) : } t_{mn}^{ae} \langle mn || be \rangle \end{array} \right\} \end{aligned} \quad (18)$$

the limitation to the second order now impose amplitudes being developed at first order

$$t_i^{a[1]} = \frac{f_i^a}{\varepsilon_i - \varepsilon_a}, \quad t_{ij}^{ab[1]} = \frac{\langle ab || ij \rangle}{\varepsilon_i + \varepsilon_j - \varepsilon_a - \varepsilon_b}, \quad (19)$$

and this obtained from MP2, so that the EOM matrix now has the form

$$\begin{pmatrix} \bar{H}_{SS}^{[2]} & \bar{H}_{SD}^{[2]} \\ \bar{H}_{DS}^{[2]} & \bar{H}_{DD}^{[2]} \end{pmatrix}. \quad (20)$$

The EOM-MBPT(2) method, though not showing a  $N^5$  scaling as in ground-state MP2, has the advantage of doing

without the iterative solution of the CCSD equations, and one only one  $N^6$  term remains (see 48). Working equations for  $\sigma$ -vectors and intermediates are given in appendix A. Finally, it is possible to combine the EOM-MBPT(2) and P-EOM approaches in the so-called P-EOM-MBPT(2) scheme, whereby the  $\bar{H}_{DD}^{[2]}$  block is further approximated to  $\bar{H}_{DD}^{[0]}$ , with  $t_i^a$  and  $t_{ij}^{ab}$  calculated as in eq. 19, or in matrix form

$$\begin{pmatrix} \bar{H}_{SS}^{[2]} & \bar{H}_{SD}^{[2]} \\ \bar{H}_{DS}^{[2]} & \bar{H}_{DD}^{[0]} \end{pmatrix}. \quad (21)$$

### III. COMPUTATIONAL DETAILS

All calculations were carried out with a development version of the DIRAC package<sup>66,67</sup>.

We employ the same geometries used in prior studies : thus, for  $\text{XO}^-$ ,  $\text{CH}_2\text{I}_2$ ,  $\text{CH}_2\text{IBr}$  and  $\text{I}_3^-$  these were taken from the work of Shee *et al.*<sup>56</sup>, whereas for HX from the study by Visscher, Styszyński, and Nieuwpoort<sup>68</sup>. We employ the dyall-av3 $\zeta$ <sup>69</sup> basis sets for the heavy elements, and Dunning's aug-cc-pVTZ<sup>70</sup> for oxygen, carbon and hydrogen. All basis sets are used uncontracted.

Unless otherwise noted, in our calculations we employ the eXact 2-Component molecular mean-field (X2Cmmf) approach<sup>71</sup>, based either on the Dirac-Coulomb ( ${}^2\text{DC}^{\text{M}}$ ) and Dirac-Coulomb-Gaunt ( ${}^2\text{DCG}^{\text{M}}$ ) Hamiltonians. For the calculations based on the  ${}^2\text{DCG}^{\text{M}}$ , two-electron integrals over small-component basis sets (SS|SS) are approximated by a point charge model<sup>72</sup>, and a Gaussian distribution is used to model the finite size of the nuclei<sup>73</sup>.

Since the size of EOM-{IP; EA; EE} matrices are generally very large due to the (2h2p/2h1p/2p1h) configurations, eigenvalues and eigenvectors are obtained using the generalization of the Davidson iterative algorithm for non-symmetric matrices<sup>56,57,74,75</sup>.

When all the spinors have been correlated during the calculations we used the notation  $[\infty E_h]$ , otherwise we follow the notation : [lower limit ; upper limit] $E_h$  to indicate, via spinor energy lower and upper bounds, the extent of the spinor space retained for the transformation from the atomic (AO) to the molecular spinor (MO) basis.

This work focuses on different halogenated systems. For the valence IPs (1h) the studied systems are  $\text{I}_3^- [-3; 12]E_h$  and  $\text{XO}^-$  with  $X \in \{\text{Cl}; \text{Br}; \text{I}; \text{At}; \text{Ts}\} [\infty E_h]$ . In all cases, the first four solutions are calculated. Then, for the potential energy curves (PECs) of the monoxides (excluding tennesine) we employed  $[-10; 100]E_h$ , and spectroscopic constants are obtained by a polynomial fit of the absolute electronic state energies for internuclear distances comprised between 1.4 Å and 2.4 Å. For core IPs, the systems studied are HCl, HBr and  $\Gamma$ , and in these cases we correlate all electrons and all virtuals ( $[\infty E_h]$ ).

For EA (1p), we considered  $\text{I}_3^-$ , for which we calculated four electronic states, and the halomethanes  $\text{CH}_2\text{I}_2$  and  $\text{CH}_2\text{IBr}$ , for which we calculated six electronic states. The correlated electrons are within the limits  $[-3; 6]E_h$  for  $\text{CH}_2\text{I}_2$  and  $[-4; 6]E_h$  for  $\text{CH}_2\text{IBr}$ .

For EE (1h1p), we present here the results obtained for the systems  $I_3^-$  and  $CH_2I_2$ . The correlated electrons are within the limits  $[-3; 12]E_h$  for  $I_3^-$  and  $[-3; 6]E_h$  for  $CH_2I_2$ .

All graphs have been prepared with Matplotlib<sup>76</sup> python library. The dataset associated with this manuscript is available at the Zenodo repository<sup>77</sup>.

## IV. RESULTS

Before beginning the discussion of our results, we introduce some shorthand notations that will be used throughout (for EE and EA a strictly analogous shorthand notations will be used) : first, IP will refer to EOM-IP-CCSD calculations whereas P-IP will refer to P-EOM-IP-CCSD calculations, and PT(2)-IP and P-PT(2)-IP will refer to the second-order perturbation theory analogues. Second, we will generally present the difference between EOM-IP-CCSD and the others approaches by  $\Delta E_{IP}$ .

In addition to these, we will provide a measure of whether electronic states are dominated by singly ionized (SI) main configuration through the notation “%SI” accompanied by percentage ranges; for example, %SI in [95%;98%] will denote the value of the square of the largest  $r_i$  coefficients in Eq. 8 falls under 0.95 and 0.98 for the states under consideration. If this value is close to 100%, a given state can be considered as monoconfigurational, and lower values will generally indicate an increased multiconfigurational character for a particular state.

Finally, we note that in what follows we will mostly focus on the comparison between theoretical approaches. The experimental data for the systems under consideration is available in the Supplementary Information.

### A. Ionization energies

#### 1. Valence ionizations, equilibrium structures

We begin our discussion on valence ionization energies with the triiodide  $I_3^-$  species. This hypervalent anion is interesting due to being one of the relatively rare molecular anions which are stable, and for the multiple pathways it offers in its photodissociation. The species has been studied theoretically<sup>56,78,79</sup> and experimentally<sup>80,81</sup>. Our results are given in table (tab.I).

We can see that overall the ionization energies obtained with the different approximate methods (collectively referred to in what follows as  $IP_{App}$ ) are very close to the reference IP value. That said, we can identify some trends for the individual approaches : we see that that P-IP generally underestimates the IP values, PT(2)-IP overestimates them, and P-PT(2)-IP falls in between. The latter, in our view, is due to a rather systematic error compensation, though we also observe that there are some non-additive effects since adding up the differences with respect to the reference for P-IP and PT(2)-IP yield results which are close, but exactly those for P-PT(2)-IP.

TABLE I: Ionization energies (IP in eV) for  $I_3^-$  employing the  ${}^2DCG^M$  Hamiltonian, and  $\Delta E_{IP}$  values for the different approximate methods considered here. The %SI in [91%;93%] for all states and methods considered.

T	IP	$\Delta E_{IP}$		
		P-IP	PT(2)-IP	P-PT(2)-IP
$IP_1^{1/2g}$	4.46	-0.05	0.11	0.06
$IP_2^{3/2g}$	5.00	-0.14	0.01	-0.10
$IP_3^{1/2u}$	4.91	-0.10	0.04	-0.03
$IP_4^{3/2u}$	4.28	-0.10	0.04	-0.04

Furthermore, we see that these four electronic states are predominantly singly ionized states (all %SI are between 91% and 93%), with the characteristic that the states are dominated by a single ionized configuration (in other words, ionizations occur from essential a single molecular orbital).

The second class of compounds for which valence ionizations were investigated is the halogen monoxides  $XO^-$  ( $X \in \{Cl; Br; I; At; Ts\}$ ). These compounds have the halogen in the (+I) oxidation state, and are for instance involved in ozone degradation<sup>82</sup> or have an interest in nuclear medicine in the case of astatine<sup>83,84</sup>. The four IP states under consideration correspond in effect to the spin-orbit split doublet ground ( ${}^2X_{1/2}, {}^2X_{3/2}$ ) and first excited ( ${}^2A_{1/2}, {}^2A_{3/2}$ ) states of the corresponding halogen monoxide radicals. As expected, as the atomic number of the halogen increases the spin-orbit splitting will be more important; Shee *et al.*<sup>56</sup> have analyzed in detail these states, and showed that the ground states are dominated by contributions from the halogen, whereas the reverse is true for the first excited state. As shown below, this will have significant implications on the performance of the approximate methods.

In figure 1 we show how  $\Delta E_{IP}$  values for the different methods vary with respect to the change in halogen for each of the spin-orbit split ground and excited states, with the size of each point being proportional of the singly ionized character for each of the electronic states (smaller sizes denoting higher 2h1p character). In general, the evolution of  $\Delta E_{IP}$  is the same for the first four solutions as we go through the excited states from the lowest to the highest: PT(2)-IP is increasing, P-IP decreasing and P-PT(2)-IP remains relatively constant across the  $XO^-$  series.

Looking closely at the different methods, we see first that for PT(2)-IP we obtain overall the smallest deviations with IP in absolute value, though we see a relatively small but clear break between chlorine, bromine and iodine on one side (which show very similar  $\Delta E_{IP}$  values for all four states), and astatine and tennesine on the other (for which  $\Delta E_{IP}$  tend to increase for the  $\Omega = 1/2$  components with respect to the  $\Omega = 3/2$  one).

For chlorine, energies are slightly overestimated for the ground state (0.06 eV) and similarly underestimated (-0.06 eV) for the  $A$  excited state. As spin-orbit coupling is very weak there are no noticeable differences in errors between the  $\Omega = 3/2$  and  $\Omega = 1/2$  components. For bromine and iodine,  $\Delta E_{IP}$  values are close to 0.11 eV, though for  $A$

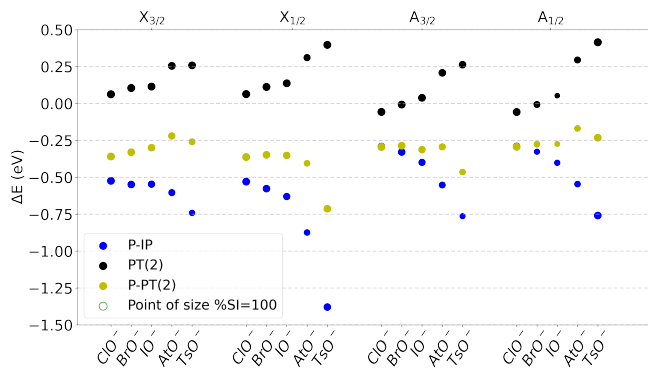


FIG. 1:  $\Delta E_{IP}$  values (in eV) for the different approximate electronic structure methods considered here as a function of electronic state and halogen. Points have a size proportional to %SI (see Supplementary Information for the list of individual ionization energy values).

these are smaller (less than 0.05 eV).

There are rather small differences in  $\Delta E_{IP}$  values for the spin-orbit splitting of the ground state (0.01 eV for bromine and 0.02 eV for iodine), and these become much smaller for the spin-orbit splitting of the  $A$  state (less than 1 meV for bromine and 0.02 eV for iodine).

Thus, for these three compounds, the average of the absolute errors  $\bar{\delta}$  for the ground state is  $\bar{\delta} = 0.1$  eV with a standard deviation of  $\sigma = 0.03$  eV, whereas for the  $A$  state, these values are  $\bar{\delta} = 0.04$  eV and  $\sigma = 0.02$  eV, strongly suggesting a systematic error. For astatine and tennessine, the error becomes larger but remains lower than 0.5 eV.

We observe that P-IP presents the worst results in terms of the absolute value of  $\Delta E_{IP}$  among all three approximations considered, and the errors being all negative means that IPs are underestimated. For the  $X_{3/2}$  state we see that the error is somewhat constant (around  $-0.5$  eV) from chlorine to iodine, and slowly increases for astatine and tennessine to reach around  $-0.75$  eV.

In qualitative terms, this is similar to what one sees for the PT(2)-IP case. For both spin-orbit split components of the excited state, we see a similar trend, but it differs slightly from PT(2)-IP case, since for the  $A_{3/2}$  state there is a larger difference between astatine and tennessine. What is remarkable in P-IP is that for  $X_{1/2}$  state there is a strong change in  $\Delta E_{IP}$  when going from astatine to tennessine, with the error reaching  $-1.38$  eV.

One element that may help understand the root of this behavior is the nature of this state: as discussed by Shee *et al.*<sup>56</sup>, in the EOM-IP-CCSD description of TsO, the  $X_{1/2}$  state is predominantly made up by a configuration with 1h character, in which  $\pi_{1/2}^*$  spinor ends up being singly occupied. However, there is also a contribution from a configuration with 2h1p character (on top of removing one electron from  $\pi_{1/2}^*$ , an electron from the doubly occupied  $\sigma_{1/2}$  is placed on the empty  $\sigma_{1/2}^*$  spinor) that is sufficiently large to affect energies by a few tenths of an eV in comparison to Fock-space coupled

cluster results<sup>56</sup>.

In such a case P-IP turns out to be poor approximation since it suppresses the ability of  $\bar{H}_{DD}$  to account for the energetics of relaxation through the 2h1p configurations, though the nature of the  $X_{1/2}$  state (spinors centered on tennessine, for which relaxation effects are potentially more important) may also play a role.

Case in point, the  $\Delta E_{IP}$  values for the  $A$  states of TsO are similar, even though EOM-IP-CCSD calculations indicate the  $A_{1/2}$  state also has a non-negligible contribution with 2h1p character (the  $\pi_{1/2}^*$  remains doubly occupied and two electrons are removed from the  $\sigma_{1/2}$  and one place on  $\sigma_{1/2}^*$ ) whereas the  $A_{3/2}$  does not. But in contrast to the  $X$  states,  $A$  states are centered on oxygen.

Finally, it turns out that the approximation of the  $\bar{H}_{DD}$  block in the P-PT(2)-IP method is compensated to some extent by the errors introduced by the approximate treatment of electron correlation. From chlorine to iodine, the differences are included in the limits:  $[-0.36; -0.27]$ eV, in this case  $\bar{\delta} = 0.34$ eV and  $\sigma = 0.02$ eV for  $X$  states and  $\bar{\delta} = 0.29$ eV,  $\sigma = 0.01$ eV for  $A$  states.

The standard deviations show us that the error is almost constant, with only the results for the  $\Omega = 1/2$  component of the ground state and to a lesser extent, the  $\Omega = 3/2$  component of the excited state of TsO deviating significantly from this trend. Paradoxically the most approximate method becomes, in this case, the most stable across the halogen monoxide series.

A final remark concerns the change in %SI for the different complexes and electronic states, shown in the Supplementary Information. We observe that there appears to be no clear cut correlation between a particular value (i.e. whether a state is mono or multiconfigurational) and the magnitude of  $\Delta E_{IP}$ .

We do note, however, that PT(2)-IP are typically very close to that of the reference calculations, whereas P-IP values are usually smaller than the reference and PT(2)-IP ones, and P-PT(2)-IP values as expected fall in between PT(2)-IP and P-IP (though tend to be closer to the latter).

Taken together, these suggest that the approximation of  $\bar{H}_{DD}$  does have a non-negligible impacts on the nature of the wavefunction by favoring an increase in multiconfigurational character for the 1h contributions.

## 2. Valence ionizations, potential energy curves

Apart from the investigation for ground-state equilibrium structures, we have also investigated the effect of the approximation on the potential energy curves for  $X$  and  $A$  states of the halogen monoxide radicals. As an example, we shown in figure 2 the results for the AtO species, as a representative of the overall trends. The curves for the other species as well as their equilibrium distances can be found in the Supplementary Information.

The first information from figure 2 is that PT(2)-IP (in black) show very good agreement to the reference values (in red) for the  $A$  states across the geometries studies. It also

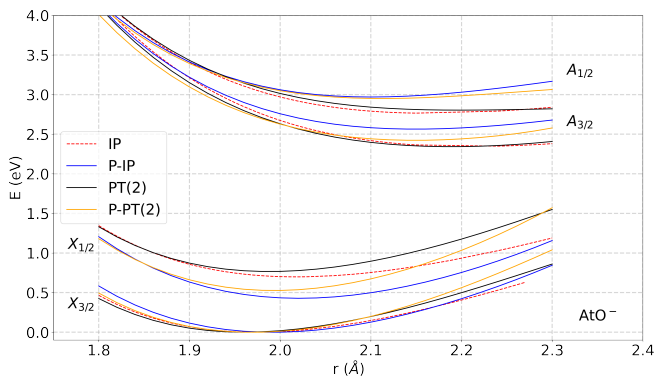


FIG. 2: Potential energy curve for AtO (in eV, shifted by the energy at the minimum of the  $X_{3/2}$  state) as function of the X-O distance ( $r$ , in Å), for the reference method and the different approximations.

reproduces rather well the curves for the X states up to the  $X_{3/2}$  equilibrium structure; for larger internuclear distances, it starts to shift towards higher energies for both spin-orbit split components, but the deviation with respect to the reference becomes more significant for the  $X_{1/2}$  state than for the  $X_{3/2}$  state.

Second, we see that the curves for the partition-based approaches (P-IP in blue and P-PT(2)-IP in yellow) are quite close to each other for internuclear distances shorter than the  $X_{3/2}$  equilibrium structure, and start to separate out for larger distances; interestingly, P-PT(2)-IP energies tend to be higher than P-IP ones for the X states, while the reverse is true for the A states.

Taken together, these results hint that for halogen monoxides P-PT(2)-IP should not necessarily be more reliable than PT(2)-IP for obtaining spectroscopic constants, or investigating excited states for geometries away from the ground-state equilibrium. But whatever the case, they provide further evidence that P-IP is the least balanced of the three approximate methods under consideration.

From the graphs it is also interesting to notice that for the  $X_{1/2}$  the P-PT(2)-IP curve goes to being closer to the P-IP curve for small internuclear distances to being closer to the PT(2)-IP for longer distances, but not for the other three states, so the error cancellation that favors the P-PT(2)-IP approach near the ground-state equilibrium structure is not uniform for different structures.

To complement this comparison we provide in figure 3 a closer look at how both energetics and equilibrium structures compare to the reference values ( $\Delta E$  and  $\Delta r$ , respectively) for the different species. From this figure we clearly see that results for P-IP are rather dispersed both in energetics and geometries.

The results for PT(2)-IP on the other hand cluster around the reference values, but not in a very homogeneous way for different species. A similar clustering is seen for P-PT(2)-IP, with the systematic error for energies which has been discussed above comparison to PT(2)-IP being clearly seen. We also observe that for chlorine, bromine and iodine, P-

PT(2)-IP results are more compactly clustered together than for PT(2)-IP (all values are included in a zone of  $\pm 0.1$  eV and  $\pm 0.025$  Å).

The difference between PT(2)-IP and IP can be explained by a poorer description of the ground state by this approximation<sup>49</sup>. A correction can be made by comparing the CCSD correlation energies with respect to MP2. We corrected our results by the difference between these two energies (relative to their respective minima) along the dissociation curve; this sometimes seems to improve the results but without a general conclusion appearing.

This compensation method can be interesting in the explanation but not very advantageous for obtaining the energies, the purpose of PT(2)-IP and P-PT(2)-IP being to avoid doing CCSD calculations. This correction could also have been made in the previous study on  $XO^-$  but a change in the baseline only leads to a change in the mean and not in the standard deviation (as the distance is fixed between the IP).

So far we have discussed the errors for the individual excited state energies, but it is also interesting to compare how the methods represent the energy differences between electronic states. If such energy differences are correctly described it becomes possible to investigate electronic transitions. Since in our discussion of the potential energy curves we have established that the errors for the different approximate methods are not constant, we restrict ourselves to a comparison around the ground-state equilibrium structure (the Franck-Condon zone).

Concerning the errors in transition energies, these are shown in figure 4; there, we take the lowest state ( $X_{3/2}$ ) as reference. As the first transition is between the spin-orbit components of the ground state, for chlorine and bromine results are essentially the same. For the two other compounds, the error increases for P-IP, for PT(2)-IP, the energies are correct and remain lower than 0.1 eV. For P-PT(2)-IP, the error remains small up to iodine for which the error is  $-0.05$  eV.

For the following two transitions ( $A_{3/2}-X_{3/2}$  and  $A_{1/2}-X_{3/2}$ ), for the same  $IP_{App}$  and the same compound, the errors are essentially the same. P-IP overestimates the energies, PT(2)-IP underestimates them but becomes more reliable for as systems become heavier (e.g. from  $ClO^-$  to  $AtO^-$ ). P-PT(2)-IP shows a more systematic behavior for the transitions between  $\Omega = 3/2$  than between  $\Omega = 3/2$  and  $\Omega = 1/2$  states.

### 3. Core ionizations

On order to avoid complexifying the notation in what follows, we will continue to employ the same acronyms for their reference and approximate methods as done for valence ionizations, but for the results all approximated methods ( $IP_{App}$ ) and the reference EOM-CCSD results (IP), it will be implicit that they were obtained the CVS approximation<sup>57</sup>.

Apart from those, since for highly symmetric systems such as HCl, HBr and  $I^-$  the DIRAC implementation can be used to carry out a complete diagonalization (that is, obtain all possible states from the EOM-CCSD matrix without invoking the

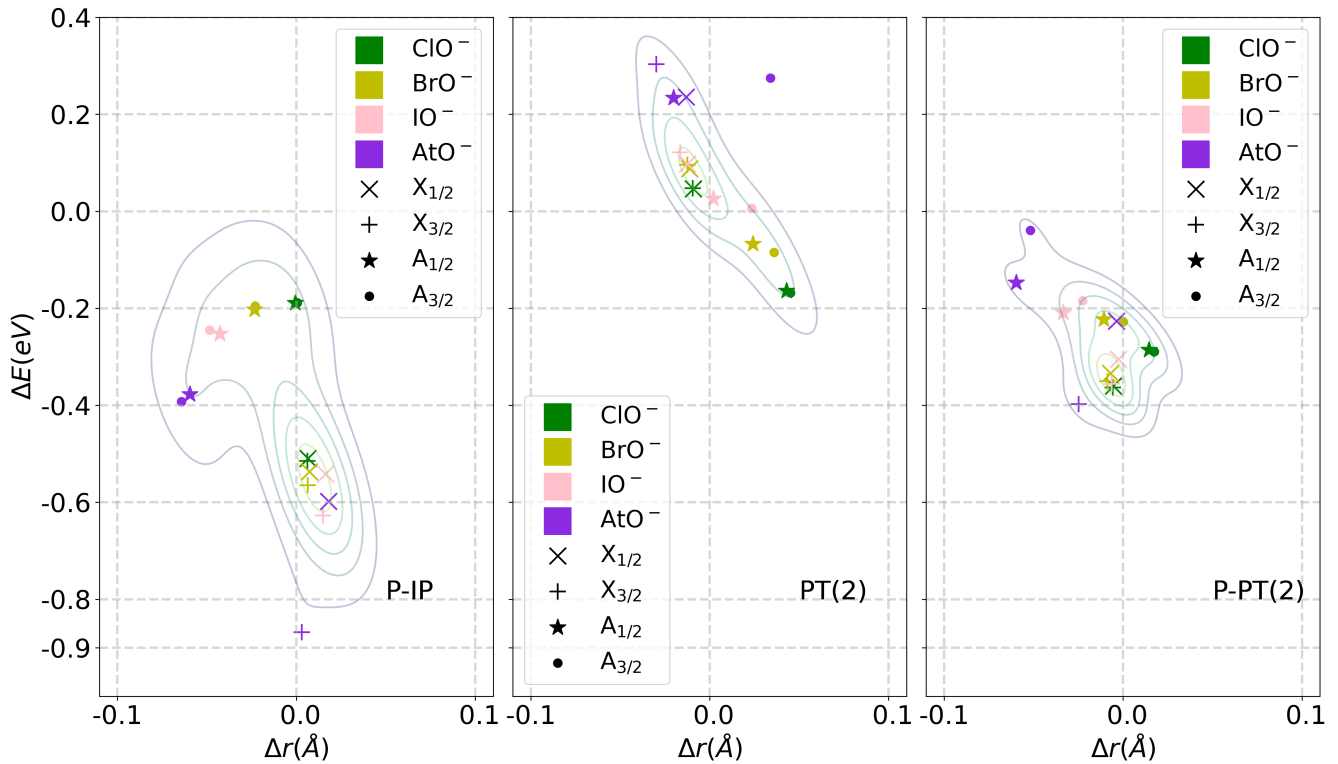


FIG. 3: Difference in the *PES* minimum positions and energies  $\Delta E$  (in eV) w.r.t.  $\Delta r$  ( $\text{\AA}$ ) for the 3  $\text{IP}_{\text{App}}$  and the 4 compounds. For reasons of readability : colors for compounds and symbols for states. The 4 different isodensities represented were calculated by a Gaussian kde algorithm<sup>85</sup>, resp. in  $[-0.1; 0.1]$  ( $\text{\AA}$ ),  $[-1.0; 0.4]$  (eV) limits for  $\Delta r$  and  $\Delta E$ .

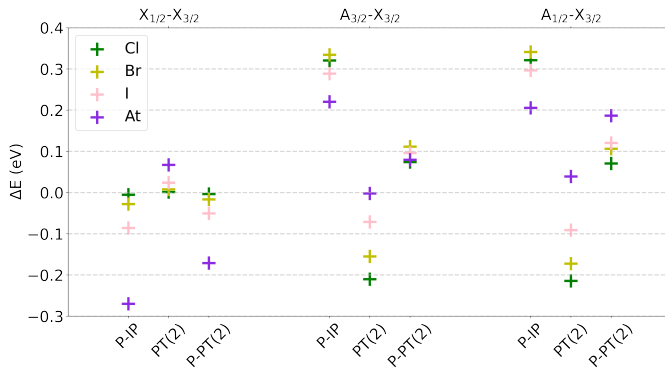


FIG. 4: Error in transition energies :  $\Delta \text{IP}_{\text{App}} - \Delta \text{IP}$  (in eV), for all  $\text{XO}^-$  and  $\text{IP}_{\text{App}}$ s (see Supplementary Information for values).

CVS approximation), we take the opportunity to present these results (denoted by the shorthand full-IP) and compare them to IP ones, thus extending our previous comparison<sup>57</sup>.

Our results are shown in table II for K- and L-edges of HCl, the M-edges of HBr, and the K-, L- and M-edges of  $\Gamma$ . In it, we present the full-IP and IP energies and their different (denoted by  $\Delta_f$ ), as well as the  $\Delta E_{IP}$  values gauging the difference between approximate methods and the reference IP results.

Before addressing the results for approximate methods, we

see from table II that the effect of the CVS approximation is rather small, with  $\Delta_f$  values being usually of a few tenths of an eV for most edges—including highly energetic ones such as the  $\Gamma$  K-edge—with a few exceptions that we had identified previously<sup>57</sup>. We also see that for molecular systems, the hydrogen-halogen bond slightly lifts the degeneracies that are expected for each of the edges if the systems were spherically symmetric, but for these systems these splittings are not particularly important. Taken together, these results attest to the reliability of the CVs approximation, for the discussion that follows.

Turning now to the performance of the approximate methods, we begin with the results HCl. We observe, for PT(2)-IP a very homogeneous error for the L-edge at around 0.13 eV, and a slightly larger error (0.23 eV) for the K-edge. For P-IP, we see errors of opposite sign compared to PT(2)-IP, indicating one more that the reference values are underestimated. More interestingly they are, in absolute value, twice as large for the K-edge, comparable for the  $L_1$ - and  $L_3(a)$ - edges, and slightly smaller for the other edges.

In the P-PT(2)-IP, we see a pattern of error cancellation which is very similar to that found for the valence ionization, though since there are much more significant differences between PT(2)-IP and P-IP for the K-edge than for the others, we see a much larger value of  $\Delta E_{IP}$ .

Moving on to HBr, we only compare the M-edge which is of similar or lower energy than the K- and L-edges of HCl. Perhaps unsurprisingly, for PT(2)-IP we see  $\Delta E_{IP}$  values with

TABLE II: Ionization energies (in eV) for HCl (K- and L-edges), HBr (M-edges) and  $\Gamma$  (K-, L- and M-edges) for the complete diagonalization of the EOM-IP-CCSD Hamiltonian (full-IP) and for the CVS approximation (IP), as well as their difference ( $\Delta_f$ , in eV). Energy differences ( $\Delta E_{IP}$ , in eV) between approximate methods and IP. We note that %SI  $IP_{App}$  are included in the range [87%; 88%], [89%; 91%] and [88%; 92%] respectively for HCl, HBr and  $\Gamma$ . The differences between labels (a), (b) and (c) denote the splitting of states due to the deviation from spherical symmetry in the presence of the hydrogen atom.

T	full-IP	CVS-IP		$\Delta E_{IP}$		
	$E_f$	$E_{IP}$	$\Delta_f$	P-IP	PT(2)-IP	P-PT(2)-IP
HCl						
$K$	2835.46	2835.76	0.30	-0.45	0.23	-0.20
$L_1$	280.25	280.27	0.02	-0.14	0.12	-0.01
$L_2$	209.66	209.59	-0.07	-0.06	0.13	0.09
$L_3(a)$	208.02	207.93	-0.09	-0.15	0.13	0.09
$L_3(b)$	207.94	207.84	-0.10	-0.06	0.13	0.08
HBr						
$M_2$	200.77	200.92	0.16	-1.15	0.15	-0.85
$M_3(a)$	194.21	194.00	-0.21	-1.13	0.15	-0.83
$M_3(b)$	194.15	193.84	-0.31	-1.13	0.14	-0.84
$M_4(a)$	78.03	78.13	0.10	-1.15	0.23	-0.78
$M_4(b)$	77.84	77.90	0.06	-1.16	0.23	-0.80
$M_5(a)$	77.00	77.05	0.06	-1.13	0.23	-0.77
$M_5(b)$	77.01	76.93	-0.08	-1.13	0.23	-0.78
$M_5(c)$	76.88	76.74	-0.13	-1.14	0.22	-0.79
$\Gamma$						
$K$	33290.63	33290.72	0.09	-5.77	1.27	-4.25
$L_1$	5209.13	5209.29	0.16	-4.35	1.02	-3.11
$L_2$	4866.09	4867.68	1.59	-4.67	1.07	-3.37
$L_3$	4567.06	4567.67	0.61	-4.53	1.06	-3.25
$M_1$	1078.43	1078.27	-0.16	-2.25	0.72	-1.41
$M_2$	937.25	936.37	0.12	-2.31	0.75	-1.44
$M_3$	878.64	878.57	-0.06	-2.21	0.74	-1.36
$M_4$	631.93	631.67	-0.26	-2.42	0.80	-1.50
$M_5$	618.89	619.81	0.91	-2.39	0.79	-1.48

are similar to, or slightly larger than those for HCl, attesting to the very systematic nature of this approximation. For P-IP we also have quite systematic errors, but they underestimate the reference more significantly than for HCl, and now in absolute value the  $\Delta E_{IP}$  are nearly 1 eV larger than for PT(2)-IP; and consequently P-PT(2)-IP are also affected and in absolute value  $\Delta E_{IP}$  are significantly larger than for PT(2)-IP.

A similar trend emerges for  $\Gamma$ , with PT(2)-IP showing a tendency to overestimate the reference (by about 1 eV), with  $\Delta E_{IP}$  which are comparable within each edge. The P-IP and PT(2)-IP approaches also show  $\Delta E_{IP}$  values which are very similar within each edge, but both show  $\Delta E_{IP}$  values which in absolute terms are significantly (between two to five times) larger than the PT(2)-IP values.

In figure 5 we provide a graphical representation of  $\Delta E_{IP}$  shown in table II above for each of the approximate methods, adding to it (red) a measure of the non-additivity (NA) of the partition and second-order approximations:

$$NA = \Delta E_{IP}(PT(2)) - [\Delta E_{IP}(P - PT(2)) - \Delta E_{IP}(P - IP)], \quad (22)$$

from which we see that there is a small non-additivity, that is slightly larger for the K and L edges with respect to the M edges.

To explain the processes behind these differences, one

should first recall that as discussed elsewhere (see e.g. Halbert *et al.*<sup>57</sup> and references therein), for the determination of core ionization energies, the contribution to the electronic states' energies of relaxation effects due to the creation of the core hole can be equally or more important than electron correlation effects South *et al.*<sup>37</sup>.

Furthermore, relaxation will be increasingly more important as one probes more energetic edges. With that, electronic structure methods that insufficiently account for relaxation (for example, using Koopmans theorem to approximate ionization energies by the absolute value of orbital energies) will in general largely overestimate core binding energies and show larger discrepancies from experiment for more energetic edges than for less energetic ones (by several tens of eV depending on the case).

Methods such as EOM-CCSD on the other hand have shown to be capable of accounting for a significant part of relaxation, and when combined with corrections for quantum electrodynamics effects and the Breit interaction are taken into account, one can obtain energies in agreement with experiment to within about 1-2 eV<sup>55,57</sup>, and show fairly constant errors for different edges.

In view of these results from the literature and our results above, in which we see fairly constant  $\Delta E_{IP}$  values for PT(2)-IP (but more energetic edges showing slightly larger values than less energetic ones), while at the same time observing a net increase in the magnitude of  $\Delta E_{IP}$  for both P-IP and P-PT(2)-IP as one goes towards (a) heavier elements; and (b) more energetic edges, we are led to the conclusion that for core ionizations PT(2)-IP does a better job at accounting for relaxation than the partition-based approaches, due to the approximation to the  $\bar{H}_{DD}$  block in the latter two.

That said, it is important to recall that all  $\Delta E_{IP}$  values shown here remain significant smaller than what would be the case if cruder approximations were employed (e.g. Koopmans theorem), meaning that these approximate methods (and in particular PT(2)-IP and P-PT(2)-IP, due to their more modest computational cost) would remain of interest for the calculation of core ionizations.

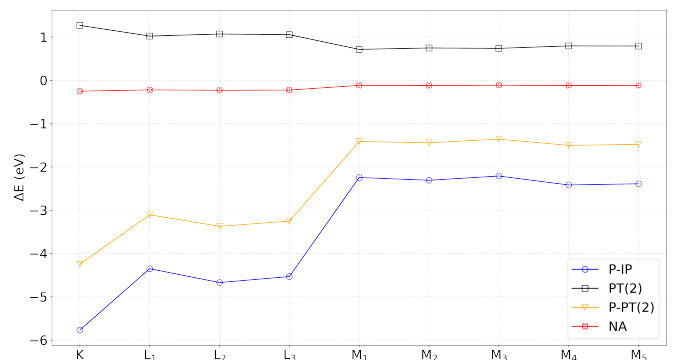


FIG. 5: Values of  $\Delta E_{IP}$  in eV for the K-, L- and M-edges of  $\Gamma$  for the PT(2)-IP, P-IP and P-PT(2)-IP approximations, as well as a measure of the non-additivity (NA) of the partition and second-order approximations.

Finally, we note that for all ionizations considered, we have %SI around [87%; 88%] for HCl, [89%; 91%] for HBr and [88%; 92%] for  $\Gamma^-$ , meaning that for all methods and systems we have been able to compare ionized states whose wavefunctions are dominated by the same ionized determinant. It is also interesting to see that for the core spectra of these species we did not see the partition-based approaches increasing the states' multideterminantal character.

## B. Electronic Affinities

Addressing now electron affinities, we summarize our results in table III. We see that for all systems considered ( $I_3^-$ ,  $CH_2IBr$  and  $CH_2I_2$ ), we have rather small and uniform errors for all approximations, so it is actually quite difficult to decide which one shows better performance as done for ionization energies. That said, we still see that PT(2)-EA still appears to be somewhat more systematic than the partition-based approaches P-EA and P-PT(2)-EA.

For these systems most electron affinities are positive and relatively large, corresponding to situation in which we have metastable states. For these cases, we see that the error introduced by the approximations are rather negligible in comparison to the electron affinities themselves.

For  $CH_2IBr$  and  $CH_2I_2$ , on the other hand, the first electron affinity is negative, denoting bound states that are nevertheless not very stable—0.03 eV for  $CH_2IBr$  and -0.33 eV for  $CH_2I_2$  respectively. We see that all of our approximated methods tend to underestimate the energies of these bound states. That makes them yield first electron attachments states which are also bound, and therefore qualitatively in line with EOM-CCSD, though slightly more stable than the latter.

These results underscore the fact that, by introducing approximations one invariably loses in accuracy, and consequently in predictive power when tiny energy differences are involved. This serves as a reminder of the importance of attempting to investigate such subtle effects with a range of methods of varying degrees of accuracy to verify whether computationally less expensive methods are sufficiently accurate.

It is noteworthy that the %SA are sometimes over 90%, but also as low as 50%, indicating the presence of at least one or more configurations, though the values are very similar across all methods for each of the individual electronic states.

## C. Excitation Energies

As a conclusion, we focus on the calculation of excitation energies with our approximate methods. Our results are reported on table IV for the triiodide  $I_3^-$  and dihalomethane  $CH_2I_2$  species.

Starting with the triiodide results, we see that our three approaches work rather well as far as the standard deviation of  $\Delta E_{EE}$  values is concerned—these are all small, meaning that that the errors for P-EE and PT(2)-EE are shifts of roughly 0.27 eV for the first (meaning it overestimates the reference

TABLE III: Electron affinities and  $\Delta E_{EA}$  values (in eV) as well as %SA values for selected low-lying states of the  $I_3^-$ ,  $CH_2IBr$  and  $CH_2I_2$  molecules.

T	EA		P-EA		PT(2)-EA		P-PT(2)-EA	
	E	%SA	%SA	$\Delta E_{EA}$	%SA	$\Delta E_{EA}$	%SA	$\Delta E_{EA}$
$I_3^-$								
EA <sub>1</sub>	2.51	76	76	-0.02	75	-0.01	74	-0.05
EA <sub>2</sub>	3.65	77	77	0.01	76	0.01	75	0.01
EA <sub>3</sub>	3.88	94	94	0.01	94	0.02	95	0.03
EA <sub>4</sub>	4.39	96	96	0.01	96	0.00	96	0.01
$CH_2IBr$								
EA <sub>1</sub>	-0.03	52	53	-0.04	52	-0.06	53	-0.08
EA <sub>2</sub>	0.45	66	70	0.00	67	-0.01	70	0.00
EA <sub>3</sub>	0.86	97	97	0.01	97	-0.01	97	0.00
EA <sub>4</sub>	0.99	87	85	0.00	86	-0.01	85	-0.01
EA <sub>5</sub>	1.62	70	69	0.01	68	-0.01	67	0.01
EA <sub>6</sub>	1.92	52	49	0.00	55	-0.01	48	0.00
$CH_2I_2$								
EA <sub>1</sub>	-0.33	48	50	-0.06	48	-0.06	49	-0.10
EA <sub>2</sub>	0.41	57	60	0.01	58	-0.01	60	0.00
EA <sub>3</sub>	0.75	83	81	-0.02	82	-0.01	80	-0.02
EA <sub>4</sub>	0.86	98	98	0.01	98	-0.01	98	0.00
EA <sub>5</sub>	1.49	87	86	0.01	86	0.00	85	0.01
EA <sub>6</sub>	1.70	67	62	-0.01	65	-0.01	61	-0.01

values) and nearly zero for the second. Due to this behavior for P-PT(2)-EE in this particular example the results are nearly identical to those of P-EE and there are no significant error cancellations, unlike the case if ionization energies.

One thing to note is that in cases in which states are nearly degenerate such as  $\{1_g; 0_u^-; 1_u\}$ , the approximate methods have a difficult time in placing them in the same order as found in EOM-CCSD (see numbers in bold on table IV). Furthermore, we note the presence of non-standard values for the first  $1_g$  and  $1_u$  by PT(2)-EE and P-PT(2)-EE. Indeed, while PT(2)-EE presents a difference of at most 0.01 eV in absolute value, the error for this level is 0.11 eV. The same is true for P-PT(2)-EE which goes from an error of 0.27 eV to 0.37 eV. These differences to EOM-CCSD are in line with limitations pointed out above for electron affinities.

Similar trends are found for  $CH_2I_2$ . For this system, standard deviations are once again satisfactory, of the order of 0.2 eV, with the averages are respectively 0.31 eV, -0.07 eV and 0.25 eV for P-EE, PT(2)-EE and P-PT(2)-EE respectively. This means that we observe very systematic but nevertheless larger overestimation P-EE, and now a slight underestimation by PT(2)-EE, which is actually the opposite trend found for ionization energies, but that means that P-PT(2)-EE again profits from error cancellation between the second-order and partition approximations. As in the case of electron affinities, we find that overall %EE values are also very similar between different approximate methods, in spite of the fluctuations from state to state.

Finally, for the comparison with CASPT(2) results for  $I_3^-$ <sup>78</sup> and  $CH_2I_2$  Liu *et al.*<sup>86</sup>, we see that in terms of the mean error the PT(2)-EE fares better than CASPT2 for both molecules, whereas P-EE and P-PT(2)-EE shows a similar behavior. However, in contrast to our methods, the  $\Delta E_{EE}$  values for CASPT2 vary much more significantly from state to state, as reflected in its much larger standard deviations.

This tendency of varying  $\Delta E_{EE}$  for different excited states

had already been identified by Gomes *et al.*<sup>78</sup> and Shee *et al.*<sup>56</sup>, but also in other benchmarks for heavy elements such as those by Tecmer *et al.*<sup>87</sup> and Tecmer *et al.*<sup>88</sup>. We consider it a significant advantage of the approximate methods over CASPT2 that former conserve such near constant difference to EOM-CCSD values, as it makes them less prone to incorrectly ordering electronic states.

TABLE IV: Excitation energies and  $\Delta E_{EE}$  values (in eV) as well as %SE values for selected low-lying excited states of the  $I_3^-$  and  $CH_2I_2$  molecules. In bold we denote electronic states whose order has been inverted in approximate calculations with respect to the reference EOM-CCSD results. Here  $\bar{x}$  and  $\sigma$  denote the mean error over all excited states considered for a particular species and the standard deviation, respectively. CASPT2 values from Gomes *et al.*<sup>78</sup> for  $I_3^-$  and from Liu *et al.*<sup>86</sup> for  $CH_2I_2$  are also provided for comparison.

T	EE		P-EE		PT(2)-EE		P-PT(2)-EE		CASPT2	
	EE	%SE	%SE	$\Delta E_{EE}$	%SE	$\Delta E_{EE}$	%SE	$\Delta E_{EE}$	E	$\Delta E_{EE}$
$I_3^-$										
$2_g$	2.25	43	45	0.27	43	0.00	45	0.27	2.24	-0.01
$1_g$	2.38	23	24	0.25	23	<b>0.11</b>	24	<b>0.37</b>	2.32	-0.06
$0_u^-$	2.38	41	42	<b>0.27</b>	41	<b>0.00</b>	42	<b>0.27</b>	2.47	0.09
$1_u$	2.38	46	47	<b>0.25</b>	46	0.11	47	0.37	2.47	0.09
$0_g^-$	2.84	21	22	0.27	22	0.00	22	0.28	2.76	-0.08
$0_g^+$	2.89	21	22	0.27	21	0.00	22	0.27	2.82	-0.07
$1_g$	3.07	41	43	0.28	41	0.01	43	0.28	2.85	-0.22
$2_g$	3.33	48	49	0.26	48	-0.01	49	0.24	3.10	-0.23
$1_u$	3.42	48	49	0.26	48	-0.01	49	0.25	3.11	-0.31
$0_u^+$	3.67	18	19	0.24	17	-0.01	19	0.23	3.52	-0.15
$2_g$	4.08	24	24	0.27	24	-0.01	24	0.26	3.98	-0.10
$0_u^-$	4.10	42	43	0.29	42	-0.01	43	0.28	3.79	-0.31
$1_g$	4.18	47	48	0.28	47	-0.01	49	0.27	4.06	-0.12
$1_u$	4.22	40	41	0.30	40	0.00	40	0.29	3.80	-0.42
$0_u^+$	4.49	15	16	0.24	15	0.00	17	0.24	4.51	0.02
$0_g^-$	4.69	20	21	0.30	20	-0.01	21	0.29	4.51	-0.18
$0_g^+$	4.70	20	21	0.30	20	-0.01	21	0.29	4.53	-0.17
$1_g$	4.90	40	36	<b>0.30</b>	40	0.01	26	<b>0.33</b>	4.60	-0.30
$\bar{x}$				0.27		0.01		0.28		-0.14
$\sigma$				0.02		0.04		0.04		0.14
$CH_2I_2$										
a	3.60	20	21	0.29	20	-0.07	21	0.23	3.76	0.16
b	3.62	20	20	0.29	20	-0.07	20	0.23	3.78	0.16
a	3.62	20	21	0.29	20	-0.06	21	0.23	3.78	0.15
b	3.84	16	17	0.30	15	-0.07	16	0.23	4.03	0.19
a	3.87	19	19	0.29	19	-0.07	19	0.23	4.27	0.40
b	3.94	13	13	0.31	12	-0.08	13	0.24	4.27	0.33
a	3.99	16	17	0.30	16	-0.08	17	0.23	4.31	0.32
b	4.06	16	16	0.31	16	-0.07	16	0.24	4.38	0.32
b	4.22	18	19	0.30	18	-0.06	19	0.25	4.50	0.28
a	4.32	15	16	0.31	15	-0.07	16	0.24	4.60	0.28
b	4.35	15	15	0.31	15	-0.06	15	0.26	4.62	0.27
a	4.49	15	15	0.31	15	-0.07	16	0.25		
b	4.63	15	15	0.33	15	-0.07	15	0.27		
a	4.68	17	17	0.35	17	-0.06	18	0.30		
b	4.74	15	14	0.34	15	-0.07	15	0.28		
a	4.91	14	15	0.36	15	-0.06	15	0.30		
$\bar{x}$				0.31		-0.07		0.25		0.26
$\sigma$				0.02		0.01		0.02		0.08

## V. CONCLUSION

In this manuscript we have detailed a pilot implementation of three approximate methods based on the relativistic EOM-CCSD method—the partitioned EOM-CCSD (P-EOM-CCSD), the second-order approximation to EOM-CCSD

(EOM-MBPT(2)) and the partitioned EOM-MBPT(2)(P-EOM-MBPT(2))—and applied them to a number of benchmark systems to assess how they compare with respect to the original EOM-CCSD for core and valence ionization, electron affinities and valence excitation energies.

These approximated methods have been shown to provide, for the most part, sufficiently accurate results with respect to the reference EOM-CCSD calculations. As a general rule, EOM-MBPT(2) has shown to overestimate reference values in a very systematic manner for ionizations and electron affinities, often by no more than a few tenths of eV for valence ionizations and somewhat less for electron affinities, and at most around 1-2 eV for core ionizations (employing the core-valence separation method). For excitation energies on the other hand it tends to slightly underestimate the EOM-CCSD results.

Conversely, the P-EOM method tends to systematically underestimate EOM-CCSD results for ionizations and electron affinities, while overestimating excitation energies. For ionizations and excitations, magnitude of the errors is in general larger than those for the EOM-MBPT(2) method, but rather similar for electron affinities. We have found however that for ionization processes in which relaxation effects brought about by 2h1p configurations are important (here, the valence ionization of tennesine monoxide, and the core ionizations of halogen-containing systems), the approximation underlying the P-EOM method (discarding all off-diagonal elements of  $\bar{H}_{DD}$  and approximating the diagonal by orbital energy differences) degrades the reliability of the method, and results differ from the reference EOM-CCSD the more such relaxation effects are important.

Because it combines both approximations, the P-EOM-MBPT(2) shows a behavior that is intermediate between EOM-MBPT(2) and P-EOM due to error cancellation. It should be said however that the method does show interesting and stable systematic errors, and will suffer less of a performance degradation than P-EOM even for cases which are particularly difficult for the latter such as the valence ionization of tennesine oxide.

Another finding is that for ionizations P-EOM, and to a lesser extent P-EOM-MBPT(2), seem to somewhat reduce the monodeterminantal nature of ionized states, compared to the EOM-CCSD and EOM-MBPT(2) calculations, though we consider these to be a consequence of the partitioned approximation rather than an underlying cause for differences in performance. This point requires investigations on a broader class of complexes, that goes beyond the scope of this work.

With respect to their behavior across different structures, our investigation of the potential energy curves for the spin-orbit split ground and first excited states of halogen monoxides shows that all of these methods have different error cancellation patterns in different regions of the potential energy curves, and therefore should be used with caution. That said, the EOM-MBPT(2) and P-EOM-MBPT(2) methods have shown to yield relatively small errors in equilibrium bond lengths for ClO, BrO and IO, with a small advantage for P-EOM-MBPT(2), though for AtO the reverse appears to be true.

With that, EOM-MBPT(2) seems to be a good first alternative to EOM-CCSD among the methods considered for carrying out exploratory calculations for valence and core properties on systems across the periodic table, followed by P-EOM-MBPT(2). On our view P-EOM does not seem to show a very interesting performance to cost ratio, especially for heavy and superheavy elements and should therefore be avoided, unless additional evidence for more molecular systems demonstrates other situations in which P-EOM fares as well or better than EOM-MBPT(2) or P-EOM-MBPT(2).

Furthermore, we observe that in the limited comparisons to CASPT2 for excitation energies, EOM-MBPT(2) shows overall better (and more systematic) agreement to EOM-CCSD while P-EOM-MBPT(2) results deviate from EOM-CCSD also in a more systematic way than CASPT2, though in absolute values their errors are comparable to CASPT2. This suggests these approximate EOM methods presented here can be viable alternatives to CASPT2 for investigating the spectroscopy of single-reference ground states.

## ACKNOWLEDGMENTS

We acknowledge support from PIA ANR project CaPPA (ANR-11-LABX-0005-01), I-SITE ULNE projects OVERSEE and MESONM International Associated Laboratory (LAI) (ANR-16-IDEX-0004), the French Ministry of Higher Education and Research, region Hauts de France council and European Regional Development Fund (ERDF), project CPER WAVETECH, and the French national supercomputing facilities (grants DARI A0090801859, A0110801859). ASPG acknowledges support from the Franco-German project CompRIXS (Agence nationale de la recherche ANR-19-CE29-0019, Deutsche Forschungsgemeinschaft JA 2329/6-1).

## Appendix A: Equations for approximated methods

Note that for the following equations : Internal summations have been omitted and  $P_-(pq)$  is a permutation operator :  $P_-(pq)g(\dots, p, q, \dots) = g(\dots, p, q, \dots) - g(\dots, q, p, \dots)$ .

As an exemple of the link between the following equations and the  $\sigma$  vector used in the Davidson procedure, and *Core-Valence-Separation* (eq.12) we have (see Shee *et al.* <sup>56</sup>):

$$\sigma_i^a = [\bar{H}_{SS}\mathcal{R}]_i^a + [\bar{H}_{SD}\mathcal{R}]_i^a \quad (\text{A1})$$

$$\sigma_{ij}^{ab} = [\bar{H}_{DS}\mathcal{R}]_{ij}^{ab} + [\bar{H}_{DD}\mathcal{R}]_{ij}^{ab} \quad (\text{A2})$$

## 1. MBPT(2) - EOM-EE

$$[\bar{H}_{SS}\mathcal{R}]_i^a = +\bar{F}_e^a r_i^e - \bar{F}_i^m r_m^a + \mathcal{W}_{ei}^{ma} r_m^e \quad (\text{A3})$$

$$[\bar{H}_{SD}\mathcal{R}]_i^a = +\bar{F}_e^m r_{mi}^{ea} + \frac{1}{2}\mathcal{W}_{ef}^{am} r_{im}^{ef} - \frac{1}{2}\mathcal{W}_{ie}^{mn} r_{mn}^{ea} \quad (\text{A4})$$

$$\begin{aligned} [\bar{H}_{DS}\mathcal{R}]_{ij}^{ab} = & -P_-(ab)\mathcal{W}_{ij}^{am} r_m^b + P_-(ij)\mathcal{W}_{ej}^{ab} r_i^e \\ & + P_-(ab) \left( V_{fe}^{bm} r_m^e \right) t_{ij}^{af} - P_-(ij) \left( V_{je}^{nm} r_m^e \right) t_{in}^{ab} \end{aligned} \quad (\text{A5})$$

$$\begin{aligned} [\bar{H}_{DD}\mathcal{R}]_{ij}^{ab} = & +P_-(ab)\bar{F}_e^b r_{ij}^{ae} - P_-(ij)\bar{F}_j^m r_{im}^{ab} \\ & + \frac{1}{2}\mathcal{W}_{ij}^{mn} r_{mn}^{ab} + P_-(ab)P_-(ij)\mathcal{W}_{ej}^{mb} r_{im}^{ae} \\ & - \frac{1}{2}P_-(ab) \left( V_{fe}^{nm} r_{mn}^{ea} \right) t_{ij}^{fb} - \frac{1}{2}P_-(ij) \left( V_{fe}^{nm} r_{jm}^{fe} \right) t_{in}^{ab} \\ & + \frac{1}{2}\mathcal{W}_{ef}^{ab} r_{ij}^{ef} \end{aligned} \quad (\text{A6})$$

## 2. MBPT(2) - EOM-IP

$$[\bar{H}_{SS}\mathcal{R}]_i = -\bar{F}_i^m r_m \quad (\text{A7})$$

$$[\bar{H}_{SD}\mathcal{R}]_i = +\bar{F}_e^m r_{mi}^e - \frac{1}{2}\mathcal{W}_{ie}^{mn} r_{nm}^e \quad (\text{A8})$$

$$[\bar{H}_{DS}\mathcal{R}]_{ij}^a = -\mathcal{W}_{ij}^{am} r_m \quad (\text{A9})$$

$$\begin{aligned} [\bar{H}_{DD}\mathcal{R}]_{ij}^a = & -P_-(ij)\bar{F}_j^m r_{im}^a + \bar{F}_e^a r_{ij}^e + \mathcal{W}_{ij}^{mn} r_{mn}^a \\ & + P_-(ij)\mathcal{W}_{ie}^{am} r_{mj}^e - \frac{1}{2} \left( V_{ef}^{mn} r_{nm}^f \right) t_{ij}^{ae} \end{aligned} \quad (\text{A10})$$

## 3. MBPT(2) - EOM-EA

$$[\bar{H}_{SS}\mathcal{R}]^a = +\bar{F}_e^a r^e \quad (\text{A11})$$

$$[\bar{H}_{SD}\mathcal{R}]^a = +\bar{F}_e^m r_m^{ea} + \frac{1}{2}\mathcal{W}_{ef}^{am} r_m^{fe} \quad (\text{A12})$$

$$[\bar{H}_{DS}\mathcal{R}]_i^{ab} = +\mathcal{W}_{ie}^{ab} r^e \quad (\text{A13})$$

$$\begin{aligned} [\bar{H}_{DD}\mathcal{R}]_i^{ab} = & +P_-(ab)\bar{F}_e^a r_i^{eb} - \bar{F}_i^m r_m^{ab} + P_-(ab)\mathcal{W}_{ie}^{am} r_m^{eb} \\ & + \frac{1}{2}\mathcal{W}_{ef}^{ab} r_i^{ef} - \frac{1}{2} \left( V_{fe}^{mn} r_n^{ef} \right) t_{im}^{ab} \end{aligned} \quad (\text{A14})$$

#### 4. MBPT(2) - EOM - Intermediates

$$\bar{F}_v^v : \bar{F}_a^e = f_a^e - f_a^m t_m^e + V_{fa}^{me} t_m^f - \frac{1}{2} V_{af}^{mn} t_{mn}^{ef} \quad (\text{A15})$$

$$\bar{F}_o^o : \bar{F}_m^i = f_m^i + f_e^i t_m^e + V_{me}^{in} t_n^e + \frac{1}{2} V_{ef}^{in} t_{mn}^{ef} \quad (\text{A16})$$

$$\mathcal{W}_{oo}^{oo} : \mathcal{W}_{mn}^{ij} = V_{mn}^{ij} + P_-(mn) V_{en}^{ij} t_m^e + \frac{1}{2} V_{ef}^{ij} t_{mn}^{ef} \quad (\text{A17})$$

$$\mathcal{W}_{vv}^{vv} : \mathcal{W}_{ef}^{ab} = V_{ef}^{ab} - P_-(ab) t_m^b V_{ef}^{am} + \frac{1}{2} t_{mn}^{ab} V_{ef}^{mn} \quad (\text{A18})$$

$$\mathcal{W}_{vo}^{ov} : \mathcal{W}_{ej}^{mb} = V_{ej}^{mb} + V_{ef}^{mb} t_j^f - V_{ej}^{mn} t_n^b - V_{ef}^{mn} \left( t_{jn}^{fb} \right) \quad (\text{A19})$$

$$\mathcal{W}_{vo}^{vv} : \mathcal{W}_{am}^{ef} = V_{am}^{ef} + P_-(ef) V_{ag}^{en} t_{mn}^{gf} + V_{ag}^{ef} t_m^g + f_a^n t_{mn}^{ef} + \frac{1}{2} V_{am}^{no} t_{no}^{ef} - P_-(ef) V_{am}^n t_n^e \quad (\text{A20})$$

$$\mathcal{W}_{oo}^{ov} : \mathcal{W}_{mn}^{ie} = V_{mn}^{ie} + f_f^i t_{mn}^{ef} - V_{mn}^{io} t_o^e + \frac{1}{2} V_{fg}^{ie} t_{mn}^{fg} + P_-(mn) V_{fn}^{ie} t_n^f + P_-(mn) V_{mf}^{io} t_{no}^{ef} \quad (\text{A21})$$

$$\bar{W}_{vo}^{ov} : \bar{W}_{ej}^{mb} = V_{ej}^{mb} - V_{nf}^{me} t_{nj}^{bf} \quad (\text{A22})$$

$$\text{MBPT(2)} \left\{ \bar{W}_{vo}^{ov} \otimes \{t_1; t_2; \hat{T}^{[1]}\} \right\} : V_{ej}^{mb} \otimes \{t_1; t_2; \hat{T}^{[1]}\} \quad (\text{A23})$$

#### 5. P-EOM

$$EE : [\bar{H}_{DD}^{[0]} \mathcal{R}]_{ij}^{ab} = P_-(ab) f_e^b r_{ij}^{ae} - P_-(ij) f_j^m r_{im}^{ab} \quad (\text{A24})$$

$$IP : [\bar{H}_{DD}^{[0]} \mathcal{R}]_{ij}^a = -P_-(ij) f_j^m r_{im}^a + f_e^a r_{ij}^e \quad (\text{A25})$$

$$EA : [\bar{H}_{DD}^{[0]} \mathcal{R}]_i^{ab} = P_-(ab) f_e^a r_i^{eb} - f_i^m r_m^{ab} \quad (\text{A26})$$

<sup>1</sup>P.-F. Loos, A. Scemama, and D. Jacquemin, "The quest for highly accurate excitation energies: A computational perspective," *The Journal of Physical Chemistry Letters* **11**, 2374–2383 (2020).

<sup>2</sup>S. I. Bokarev and O. Kühn, "Theoretical X-Ray spectroscopy of transition metal compounds," *WIREs Computational Molecular Science* **10**, – (2019).

<sup>3</sup>R. Izsák, "Single-reference coupled cluster methods for computing excitation energies in large molecules: The efficiency and accuracy of approximations," *WIREs Computational Molecular Science* **10**, – (2019).

<sup>4</sup>N. V. Alov, "Fifty years of X-Ray photoelectron spectroscopy," *Journal of Analytical Chemistry* **60**, 297–300 (2005).

<sup>5</sup>C. S. Fadley, "X-Ray photoelectron spectroscopy: Progress and perspectives," *Journal of Electron Spectroscopy and Related Phenomena* **178-179**, 2–32 (2010).

<sup>6</sup>J. Doucet and J. Baruchel, "Rayonnement synchrotron et applications," *CND : méthodes globales et volumiques* (2016), 10.51257/a-v3-p2700.

<sup>7</sup>M.-E. Couprie, "New generation of light sources: Present and future," *Journal of Electron Spectroscopy and Related Phenomena* **196**, 3–13 (2014).

<sup>8</sup>U. Bergmann, V. Yachandra, and J. Yano, eds., *X-Ray Free Electron Lasers: Applications in Materials, Chemistry and Biology*, Energy and Environment Series No. 18 (Royal Society of Chemistry, 2017).

<sup>9</sup>L. Young, K. Ueda, M. Gühr, P. H. Bucksbaum, M. Simon, S. Mukamel, N. Rohringer, K. C. Prince, C. Masciovecchio, M. Meyer, A. Rudenko, D. Rolles, C. Bostedt, M. Fuchs, D. A. Reis, R. Santra, H. Kapteyn, M. Murnane, H. Ibrahim, F. Légaré, M. Vrakking, M. Isinger, D. Kroon,

M. Gisselbrecht, A. L'Huillier, H. J. Wörner, and S. R. Leone, "Roadmap of ultrafast X-Ray atomic and molecular physics," *Journal of Physics B: Atomic, Molecular and Optical Physics* **51**, 032003 (2018).

<sup>10</sup>F. Gunzer, S. Krüger, and J. Grotemeyer, "Photoionization and photofragmentation in mass spectrometry with visible and UV lasers," *Mass Spectrometry Reviews* **38**, 202–217 (2018).

<sup>11</sup>J. C. Rienstra-Kiracofe, G. S. Tschumper, H. F. Schaefer, S. Nandi, and G. B. Ellison, "Atomic and molecular electron affinities: photoelectron experiments and theoretical computations," *Chemical Reviews* **102**, 231–282 (2002).

<sup>12</sup>R. M. Richard, M. S. Marshall, O. Dolgounitcheva, J. V. Ortiz, J.-L. Brédas, N. Marom, and C. D. Sherrill, "Accurate ionization potentials and electron affinities of acceptor molecules I. reference data at the CCSD(T) complete basis set limit," *Journal of Chemical Theory and Computation* **12**, 595–604 (2016).

<sup>13</sup>D. Chakraborty and D. Nandi, "Absolute dissociative electron attachment cross-section measurement of difluoromethane," *Physical Review A* **102**, – (2020).

<sup>14</sup>G. Grell, S. I. Bokarev, B. Winter, R. Seidel, E. F. Aziz, S. G. Aziz, and O. Kühn, "Multi-reference approach to the calculation of photoelectron spectra including spin-orbit coupling," *The Journal of Chemical Physics* **143**, 074104 (2015).

<sup>15</sup>M. Lundberg and M. G. Delcey, "Multiconfigurational approach to X-Ray spectroscopy of transition metal complexes," in *Transition Metals in Coordination Environments* (Springer International Publishing, 2019) pp. 185–217.

<sup>16</sup>D. Maganas, J. K. Kowalska, M. Nooijen, S. DeBeer, and F. Neese, "Comparison of multireference ab initio wavefunction methodologies for X-Ray absorption edges: A case study on  $[\text{Fe}(\text{II/III})\text{Cl}_4]^{2-/1-}$  molecules," *The Journal of Chemical Physics* **150**, 104106 (2019).

<sup>17</sup>N. A. Besley, "Density Functional Theory Based Methods for the Calculation of X-Ray Spectroscopy," *Accounts of Chemical Research* **53**, 1306–1315 (2020).

<sup>18</sup>N. A. Besley, "Modeling of the spectroscopy of core electrons with density functional theory," *WIREs Computational Molecular Science* , – (2021).

<sup>19</sup>B. Brena and Y. Luo, "Time-dependent DFT calculations of core electron shake-up states of metal-(free)-phthalocyanines," *Radiation Physics and Chemistry* **75**, 1578–1581 (2006).

<sup>20</sup>A. E. A. Fouda and N. A. Besley, "Assessment of basis sets for density functional theory-based calculations of core-electron spectroscopies," *Theoretical Chemistry Accounts* **137** (2017), 10.1007/s00214-017-2181-0.

<sup>21</sup>M. D. Santis, V. Vallet, and A. S. P. Gomes, "Environment effects on x-ray absorption spectra with quantum embedded real-time time-dependent density functional theory approaches," *Frontiers in Chemistry* **10**, – (2022).

<sup>22</sup>A. Dreuw and M. Wormit, "The algebraic diagrammatic construction scheme for the polarization propagator for the calculation of excited states," *Wiley Interdisciplinary Reviews: Computational Molecular Science* **5**, 82–95 (2014).

<sup>23</sup>J. Wenzel, M. Wormit, and A. Dreuw, "Calculating core-level excitations and X-Ray absorption spectra of medium-sized closed-shell molecules with the algebraic-diagrammatic construction scheme for the polarization propagator," *Journal of Computational Chemistry* **35**, 1900–1915 (2014).

<sup>24</sup>H. Koch, H. J. A. Jensen, P. Jørgensen, and T. Helgaker, "Excitation energies from the coupled cluster singles and doubles linear response function (CCSDLR). applications to Be,  $\text{CH}^+$ , CO, and  $\text{H}_2\text{O}$ ," *The Journal of Chemical Physics* **93**, 3345–3350 (1990).

<sup>25</sup>S. Coriani and H. Koch, "Communication: X-Ray absorption spectra and core-ionization potentials within a core-valence separated coupled cluster framework," *The Journal of Chemical Physics* **143**, 181103 (2015).

<sup>26</sup>R. J. Bartlett and M. Musiał, "Coupled-cluster theory in quantum chemistry," *Reviews of Modern Physics* **79**, 291–352 (2007).

<sup>27</sup>S. Coriani, O. Christiansen, T. Fransson, and P. Norman, "Coupled-Cluster Response Theory for Near-Edge X-Ray-Absorption Fine Structure of Atoms and Molecules," *Phys. Rev. A* **85**, 022507 (2012).

<sup>28</sup>A. Sadybekov and A. I. Krylov, "Coupled-cluster based approach for core-ionized and core-excited states in condensed phase: Theory and application to different protonated forms of aqueous glycine," *J. Chem. Phys.* **147**, 014107 (2017).

<sup>29</sup>M. L. Vidal, X. Feng, E. Epifanovsky, A. I. Krylov, and S. Coriani, "New and efficient equation-of-motion coupled-cluster framework for core-

- excited and core-ionized states,” *J. Chem. Theory Comput.* **15**, 3117–3133 (2019).
- <sup>30</sup>B. Peng, P. J. LeStrange, J. J. Goings, M. Caricato, and X. Li, “Energy-Specific Equation-of-Motion Coupled-Cluster Methods for High-Energy Excited States: Application to K-Edge X-Ray Absorption Spectroscopy,” *J. Chem. Theory Comput.* **11**, 4146 (2015).
- <sup>31</sup>Y. C. Park, A. Perera, and R. J. Bartlett, “Equation of motion coupled-cluster for core excitation spectra: Two complementary approaches,” *J. Chem. Phys.* **151**, 164117 (2019).
- <sup>32</sup>D. A. Matthews, “EOM-CC methods with approximate triple excitations applied to core excitation and ionisation energies,” *Mol. Phys.* **118**, e1771448 (2020).
- <sup>33</sup>P. S. Bagus, “Self-consistent-field wave functions for hole states of some Ne-like and Ar-like ions,” *Physical Review* **139**, A619–A634 (1965).
- <sup>34</sup>P. S. Bagus, F. Illas, G. Pacchioni, and F. Parmigiani, “Mechanisms responsible for chemical shifts of core-level binding energies and their relationship to chemical bonding,” *Journal of Electron Spectroscopy and Related Phenomena* **100**, 215–236 (1999).
- <sup>35</sup>A. Naves de Brito, N. Correia, S. Svensson, and H. Ågren, “A theoretical study of X-Ray photoelectron spectra of model molecules for polymethylmethacrylate,” *The Journal of Chemical Physics* **95**, 2965–2974 (1991).
- <sup>36</sup>J. Shim, M. Klobukowski, M. Barysz, and J. Leszczynski, “Calibration and applications of the  $\Delta$ mp2 method for calculating core electron binding energies,” *Physical Chemistry Chemical Physics* **13**, 5703 (2011).
- <sup>37</sup>C. South, A. Shee, D. Mukherjee, A. K. Wilson, and T. Saue, “4-component relativistic calculations of  $L_3$  ionization and excitations for the isoelectronic species  $UO_2^{2+}$ ,  $OUN^+$  and  $UN_2$ ,” *Physical Chemistry Chemical Physics* **18**, 21010–21023 (2016).
- <sup>38</sup>N. A. Besley, A. T. B. Gilbert, and P. M. W. Gill, “Self-consistent-field calculations of core excited states,” *The Journal of Chemical Physics* **130**, 124308 (2009).
- <sup>39</sup>N. Pueyo Bellafont, P. S. Bagus, and F. Illas, “Prediction of core level binding energies in density functional theory: Rigorous definition of initial and final state contributions and implications on the physical meaning of kohnsham energies,” *The Journal of Chemical Physics* **142**, 214102 (2015).
- <sup>40</sup>Y. Takahata and D. P. Chong, “DFT calculation of core- and valence-shell electron excitation and ionization energies of 2, 1, 3-benzo thiazole  $C_6H_4SN_2$ , 1, 3, 2, 4-benzodithiadiazine  $C_6H_4S_2N_2$ , and 1, 3, 5, 2, 4-benzotrithiadiazepine  $C_6H_4S_3N_2$ ,” *Journal of Electron Spectroscopy and Related Phenomena* **185**, 475–485 (2012).
- <sup>41</sup>J. D. Watts and R. J. Bartlett, “The coupled-cluster single, double, and triple excitation model for open-shell single reference functions,” *The Journal of Chemical Physics* **93**, 6104–6105 (1990).
- <sup>42</sup>X. Zheng and L. Cheng, “Performance of delta-coupled-cluster methods for calculations of core-ionization energies of first-row elements,” *Journal of Chemical Theory and Computation* **15**, 4945–4955 (2019).
- <sup>43</sup>M. Nooijen and R. J. Bartlett, “Equation of motion coupled cluster method for electron attachment,” *The Journal of Chemical Physics* **102**, 3629–3647 (1995).
- <sup>44</sup>J. J. Goings, M. Caricato, M. J. Frisch, and X. Li, “Assessment of low-scaling approximations to the equation of motion coupled-cluster singles and doubles equations,” *The Journal of Chemical Physics* **141**, 164116 (2014).
- <sup>45</sup>A. K. Dutta, J. Gupta, H. Pathak, N. Vaval, and S. Pal, “Partitioned EOMEA-MBPT(2): An efficient  $n^5$  scaling method for calculation of electron affinities,” *Journal of Chemical Theory and Computation* **10**, 1923–1933 (2014).
- <sup>46</sup>A. K. Dutta, N. Vaval, and S. Pal, “Lower scaling approximation to EOM-CCSD: A critical assessment of the ionization problem,” *International Journal of Quantum Chemistry* **118**, e25594 (2018).
- <sup>47</sup>M. Nooijen and J. G. Snijders, “Second order many-body perturbation approximations to the coupled cluster green’s function,” *The Journal of Chemical Physics* **102**, 1681–1688 (1995).
- <sup>48</sup>J. F. Stanton and J. Gauss, “Perturbative treatment of the similarity transformed hamiltonian in equation-of-motion coupled-cluster approximations,” *The Journal of Chemical Physics* **103**, 1064–1076 (1995).
- <sup>49</sup>S. R. Gwaltney, M. Nooijen, and R. J. Bartlett, “Simplified methods for equation-of-motion coupled-cluster excited state calculations,” *Chemical Physics Letters* **248**, 189–198 (1996).
- <sup>50</sup>M. Nooijen, S. A. Perera, and R. J. Bartlett, “Partitioned equation-of-motion coupled cluster approach to indirect nuclear spin-spin coupling constants,” *Chemical Physics Letters* **266**, 456–464 (1997).
- <sup>51</sup>T. Saue, K. Faegri, Jr., T. Helgaker, and O. Gropen, “Principles of direct 4-component relativistic SCF: application to caesium auride,” *Molecular Physics* **91**, 937–950 (1997).
- <sup>52</sup>P. Pyykkö and J. P. Desclaux, “Relativity and the periodic system of elements,” *Accounts of Chemical Research* **12**, 276–281 (1979).
- <sup>53</sup>P. Pyykkö, “Relativistic effects in structural chemistry,” *Chemical Reviews* **88**, 563–594 (1988).
- <sup>54</sup>P. Pyykkö, “The physics behind chemistry and the periodic table,” *Chemical Reviews* **112**, 371–384 (2011).
- <sup>55</sup>R. A. Opoku, C. Toubin, and A. S. P. Gomes, “Simulating core electron binding energies of halogenated species adsorbed on ice surfaces and in solution *via* relativistic quantum embedding calculations,” *Physical Chemistry Chemical Physics* **24**, 14390–14407 (2022).
- <sup>56</sup>A. Shee, T. Saue, L. Visscher, and A. S. P. Gomes, “Equation-of-motion coupled-cluster theory based on the 4-component dirac-coulomb(-gaunt) hamiltonian. energies for single electron detachment, attachment, and electronically excited states,” *The Journal of Chemical Physics* **149**, 174113 (2018).
- <sup>57</sup>L. Halbert, M. L. Vidal, A. Shee, S. Coriani, and A. S. P. Gomes, “Relativistic EOM-CCSD for core-excited and core-ionized state energies based on the four-component dirac-coulomb(-gaunt) hamiltonian,” *Journal of Chemical Theory and Computation* **17**, 3583–3598 (2021).
- <sup>58</sup>A. Saiz-Lopez, J. M. C. Plane, A. R. Baker, L. J. Carpenter, R. von Glasow, J. C. G. Martin, G. McFiggans, and R. W. Saunders, “Atmospheric chemistry of iodine,” *Chemical Reviews* **112**, 1773–1804 (2011).
- <sup>59</sup>G. Steinhauser, A. Brandl, and T. E. Johnson, “Comparison of the chernobyl and fukushima nuclear accidents: A review of the environmental impacts,” *Science of The Total Environment* **470-471**, 800–817 (2014).
- <sup>60</sup>T. D. Crawford and H. F. Schaefer, “An introduction to coupled cluster theory for computational chemists,” in *Reviews in Computational Chemistry* (John Wiley & Sons, Inc., 2007) pp. 33–136.
- <sup>61</sup>L. S. Cederbaum, W. Domcke, and J. Schirmer, “Many-body theory of core holes,” *Physical Review A* **22**, 206–222 (1980).
- <sup>62</sup>P.-O. Löwdin, “Studies in perturbation theory,” *Journal of Molecular Spectroscopy* **10**, 12–33 (1963).
- <sup>63</sup>K. P. Lawley, ed., *Ab initio methods in quantum chemistry*, Advances in chemical physics No. v. 67, 69 (Wiley, Chichester [West Sussex] ; New York, 1987).
- <sup>64</sup>J. Geertsen, M. Rittby, and R. J. Bartlett, “The equation-of-motion coupled-cluster method: Excitation energies of be and CO,” *Chemical Physics Letters* **164**, 57–62 (1989).
- <sup>65</sup>J. Gauss and J. F. Stanton, “Coupled-cluster calculations of nuclear magnetic resonance chemical shifts,” *The Journal of Chemical Physics* **103**, 3561–3577 (1995).
- <sup>66</sup>(2019), DIRAC, a relativistic ab initio electronic structure program, Release DIRAC19 (2019), written by A. S. P. Gomes, T. Saue, L. Visscher, H. J. Aa. Jensen, and R. Bast, with contributions from I. A. Aucar, V. Bakken, K. G. Dyall, S. Dubillard, U. Ekström, E. Eliav, T. Enevoldsen, E. Faßhauer, T. Fleig, O. Fossgaard, L. Halbert, E. D. Hedegård, B. Helmlich-Paris, T. Helgaker, J. Henriksson, M. Iliáš, Ch. R. Jacob, S. Knecht, S. Komorovský, O. Kullie, J. K. Lærdahl, C. V. Larsen, Y. S. Lee, H. S. Nataraj, M. K. Nayak, P. Norman, G. Olejniczak, J. Olsen, J. M. H. Olsen, Y. C. Park, J. K. Pedersen, M. Pernpointner, R. di Remigio, K. Ruud, P. Salek, B. Schimmelpfennig, B. Senjean, A. Shee, J. Sikkema, A. J. Thorvaldsen, J. Thyssen, J. van Stralen, M. L. Vidal, S. Villaume, O. Visser, T. Winther, and S. Yamamoto (available at <http://dx.doi.org/10.5281/zenodo.3572669>, see also <http://www.diracprogram.org>).
- <sup>67</sup>T. Saue, R. Bast, A. S. P. Gomes, H. J. A. Jensen, L. Visscher, I. A. Aucar, R. D. Remigio, K. G. Dyall, E. Eliav, E. Fasshauer, T. Fleig, L. Halbert, E. D. Hedegård, B. Helmlich-Paris, M. Iliáš, C. R. Jacob, S. Knecht, J. K. Lærdahl, M. L. Vidal, M. K. Nayak, M. Olejniczak, J. M. H. Olsen, M. Pernpointner, B. Senjean, A. Shee, A. Sunaga, and J. N. P. van Stralen, “The DIRAC code for relativistic molecular calculations,” *The Journal of Chemical Physics* **152**, 204104 (2020).
- <sup>68</sup>L. Visscher, J. Styszyński, and W. C. Nieuwpoort, “Relativistic and correlation effects on molecular properties. II. the hydrogen halides HF, HCl, HBr, HI, and HAT,” *The Journal of Chemical Physics* **105**, 1987–1994 (1996).

- <sup>69</sup>K. G. Dyall, "Relativistic quadruple-zeta and revised triple-zeta and double-zeta basis sets for the 4p, 5p, and 6p elements," *Theoretical Chemistry Accounts* **115**, 441–447 (2006).
- <sup>70</sup>R. A. Kendall, T. H. Dunning, and R. J. Harrison, "Electron affinities of the first-row atoms revisited. systematic basis sets and wave functions," *The Journal of Chemical Physics* **96**, 6796–6806 (1992).
- <sup>71</sup>J. Sikkema, L. Visscher, T. Saue, and M. Iliaš, "The molecular mean-field approach for correlated relativistic calculations," *The Journal of Chemical Physics* **131**, 124116 (2009).
- <sup>72</sup>L. Visscher, "Approximate molecular relativistic dirac-coulomb calculations using a simple coulombic correction," *Theoretical Chemistry Accounts: Theory, Computation, and Modeling (Theoretica Chimica Acta)* **98**, 68–70 (1997).
- <sup>73</sup>L. Visscher and K. G. Dyall, "Dirac-fock atomic electronic structure calculations using different nuclear charge distributions," *Atomic Data and Nuclear Data Tables* **67**, 207–224 (1997).
- <sup>74</sup>E. R. Davidson, "The iterative calculation of a few of the lowest eigenvalues and corresponding eigenvectors of large real-symmetric matrices," *Journal of Computational Physics* **17**, 87–94 (1975).
- <sup>75</sup>K. Hirao and H. Nakatsuji, "A generalization of the davidson's method to large nonsymmetric eigenvalue problems," *Journal of Computational Physics* **45**, 246–254 (1982).
- <sup>76</sup>J. D. Hunter, "Matplotlib: A 2d graphics environment," *Computing in Science & Engineering* **9**, 90–95 (2007).
- <sup>77</sup>L. Halbert and A. Severo Pereira Gomes, "Dataset: The performance of approximate equation of motion coupled cluster for valence and core states of heavy element systems," (2023).
- <sup>78</sup>A. S. P. Gomes, L. Visscher, H. Bolvin, T. Saue, S. Knecht, T. Fleig, and E. Eliav, "The electronic structure of the triiodide ion from relativistic correlated calculations: A comparison of different methodologies," *The Journal of Chemical Physics* **133**, 064305 (2010).
- <sup>79</sup>Z. Wang, Z. Tu, and F. Wang, "Equation-of-motion coupled-cluster theory for excitation energies of closed-shell systems with spin-orbit coupling," *Journal of Chemical Theory and Computation* **10**, 5567–5576 (2014).
- <sup>80</sup>L. Zhu, K. Takahashi, M. Saeki, T. Tsukuda, and T. Nagata, "Photodissociation of gas-phase  $I_3^-$ : product branching in the visible and UV regions," *Chemical Physics Letters* **350**, 233–239 (2001).
- <sup>81</sup>H. Choi, R. T. Bise, A. A. Hoops, and D. M. Neumark, "Photodissociation dynamics of the triiodide anion ( $I_3^-$ )," *The Journal of Chemical Physics* **113**, 2255–2262 (2000).
- <sup>82</sup>J. B. Burkholder, R. A. Cox, and A. R. Ravishankara, "Atmospheric degradation of ozone depleting substances, their substitutes, and related species," *Chemical Reviews* **115**, 3704–3759 (2015).
- <sup>83</sup>L. Liu, *Exploration of astatine chemistry in solution : focus on the Pourbaix diagram in noncomplexing medium and characterization of astatine-mediated halogen bonds*, Theses, Ecole nationale supérieure Mines-Télécom Atlantique (2020).
- <sup>84</sup>G. Vaidyanathan and M. Zalutsky, "Astatine radiopharmaceuticals: Prospects and problems," *Current Radiopharmaceuticals* **1**, 177–196 (2008).
- <sup>85</sup>"Scipy representation of a kernel density estimate using gaussian kernels," [https://docs.scipy.org/doc/scipy/reference/generated/scipy.stats.gaussian\\_kde.html](https://docs.scipy.org/doc/scipy/reference/generated/scipy.stats.gaussian_kde.html), accessed: 2023-07-01.
- <sup>86</sup>Y.-J. Liu, L. D. Vico, R. Lindh, and W.-H. Fang, "Spin-orbit ab initio investigation of the ultraviolet photolysis of diiodomethane," *ChemPhysChem* **8**, 890–898 (2007).
- <sup>87</sup>P. Tecmer, A. S. P. Gomes, U. Ekström, and L. Visscher, "Electronic spectroscopy of  $UO_2^{2+}$ ,  $NUO^+$  and  $NUN$ : an evaluation of time-dependent density functional theory for actinides," *Physical Chemistry Chemical Physics* **13**, 6249 (2011).
- <sup>88</sup>P. Tecmer, A. S. P. Gomes, S. Knecht, and L. Visscher, "Communication: Relativistic fock-space coupled cluster study of small building blocks of larger uranium complexes," *The Journal of Chemical Physics* **141**, 041107 (2014).

# Supplementary information: The performance of approximate equation of motion coupled cluster for valence and core states of heavy element systems

Loic Halbert<sup>1, a)</sup> and André Severo Pereira Gomes<sup>1, b)</sup>

Université de Lille, CNRS, UMR 8523—PhLAM—Physique des Lasers Atomes et Molécules, F-59000 Lille, France

## I. SUPPLEMENTARY INFORMATION

### A. Introduction

Here again for table :

- P-EE; P-IP; P-EA: partitioned EOM- $\{EE; IP; EA\}$
- PT(2): Many Body Perturbation Theory(2)
- P-PT(2): partitioned Many Body Perturbation Theory(2)

Finally, remember that : for the  $k^{\text{th}}$  solution, with  $(r_i)_k$  of the determinant 'single ionization'  $|\Phi_i\rangle$ , we then define :  $\%SI = 100((r_i)_k)^2$ . Likewise, we define :  $\%SA = 100((r_i^a)_k)^2$  and  $\%SE = 100((r_i^a)_k)^2$ .

### B. HCl-HBr in CVS

For HCl and HBr : as the full diagonalisation was available for these compounds, the comparison is made, first, CVS w.r.t. the full diagonalisation. Then, *full diagonalisation-Approximated methods* w.r.t. full diagonalisation is shown.

TABLE I: Energy 'E' (in eV) and the  $\%SI = 100((r_i)_k)^2$  of the selected solution for HCl.  $\Delta_f$  is the difference w.r.t. full-IP and  $\Delta_{IP}$  is the difference  $IP_{\text{App}}-IP$ . 'mean' and 'std' for the L edge, respectively : the mean and the standard deviation of the difference in energie. For experimental data precision of  $\pm 0.5$  eV.

T	full-IP		IP		P-IP			PT(2)			P-PT(2)			full-P-IP		full-PT(2)		full-P-PT(2)		exp
	$E_f$	%SI	$\Delta_f$	%SI	$\Delta_f$	$\Delta_{IP}$	%SI	$\Delta_f$	$\Delta_{IP}$	%SI	$\Delta_f$	$\Delta_{IP}$	%SI	$\Delta_f$	%SI	$\Delta_f$	%SI	$\Delta_f$	%SI	
K	2835.464	86	0.300	88	-0.153	-0.453	88	0.524	0.225	88	0.096	-0.203	88	-0.137	88	0.223	87	0.112	88	
$L_1$	280.254	12	0.018	89	-0.123	-0.140	88	0.136	0.118	89	0.010	-0.008	88	-0.216	19	0.007	14	-0.164	34	
$L_2$	209.661	87	-0.074	88	-0.132	-0.057	87	0.055	0.130	88	0.012	0.086	88	0.047	78	0.125	87	0.172	80	209.01 <sup>?</sup> ; 208.6 <sup>?</sup>
$L_3(a)$	208.016	87	-0.088	88	-0.148	-0.059	87	0.042	0.131	88	-0.003	0.085	88	-0.257	1	0.126	87	-0.146	2	207.1 <sup>?</sup>
$L_3(b)$	207.936	86	-0.100	88	-0.162	-0.063	88	0.027	0.127	88	-0.021	0.078	88	-0.417	65	0.119	87	-0.314	61	207.38 <sup>?</sup>
mean(L)			-0.0612		-0.1412	-0.800		0.065	0.127		-0.001	0.061		-0.211		0.094		-0.113		
std (L)			0.0465		0.0152	0.035		0.042	0.005		0.013	0.040		0.149		0.045		0.158		

<sup>a)</sup>Electronic mail: loic.halbert@univ-lille.fr

<sup>b)</sup>Electronic mail: andre.gomes@univ-lille.fr

FIG. 1: Energies (in eV) for HCl - Comparison between CVS IP<sub>App</sub>s and full-IP for the K and L edges for the 2 upper graph, for the two second it is the comparison between IP<sub>App</sub>s full diagonalized and full-IP, all values in eV. The points have a size proportional to  $\%SI = 100 \left( \frac{r_i}{r_k} \right)^2$ , to compare, in the first block, the green circle corresponds to a %SI of 100%. Experimental data  $\dagger?$ ;  $\dagger\dagger?$  are given with error bars.

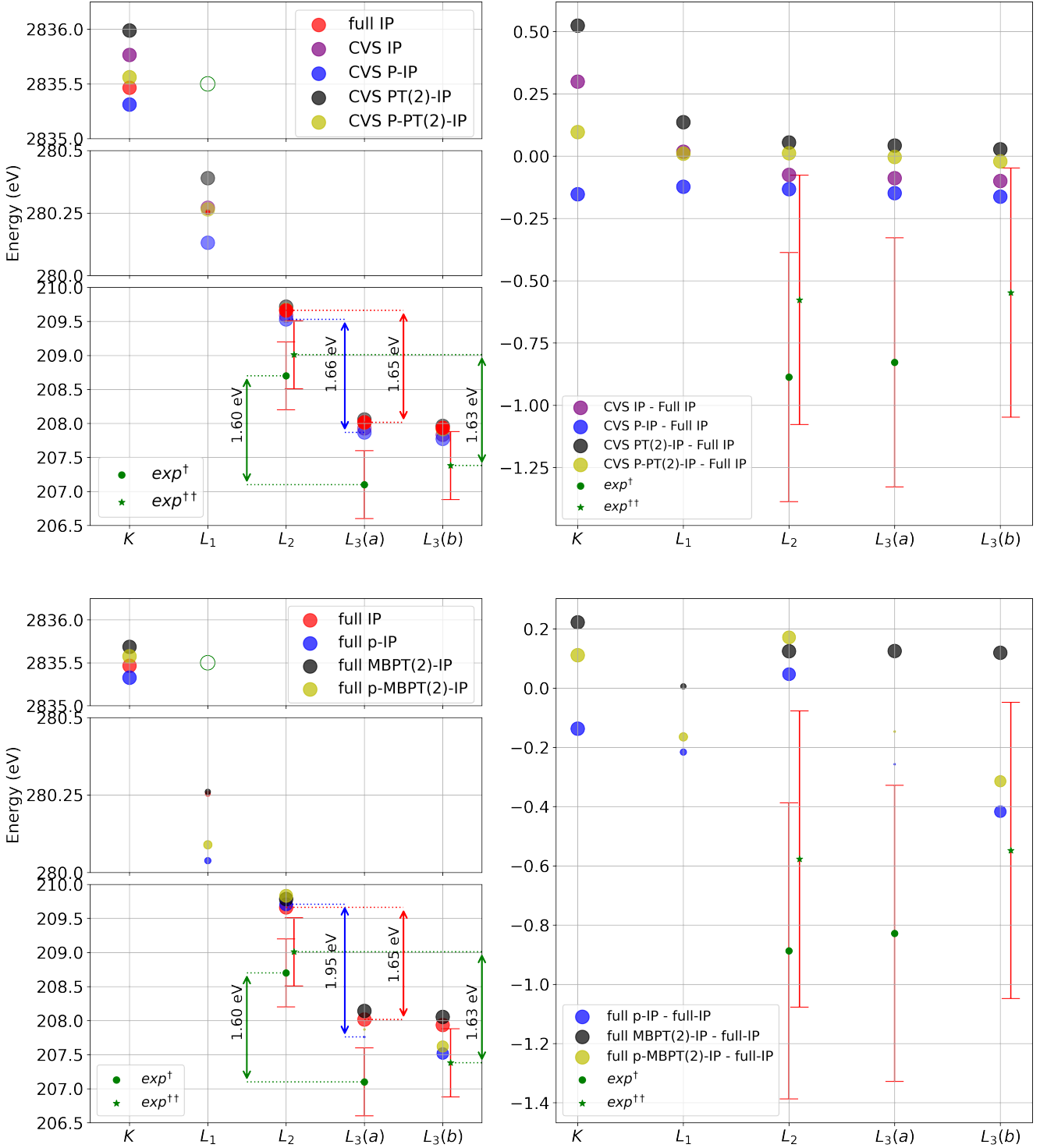
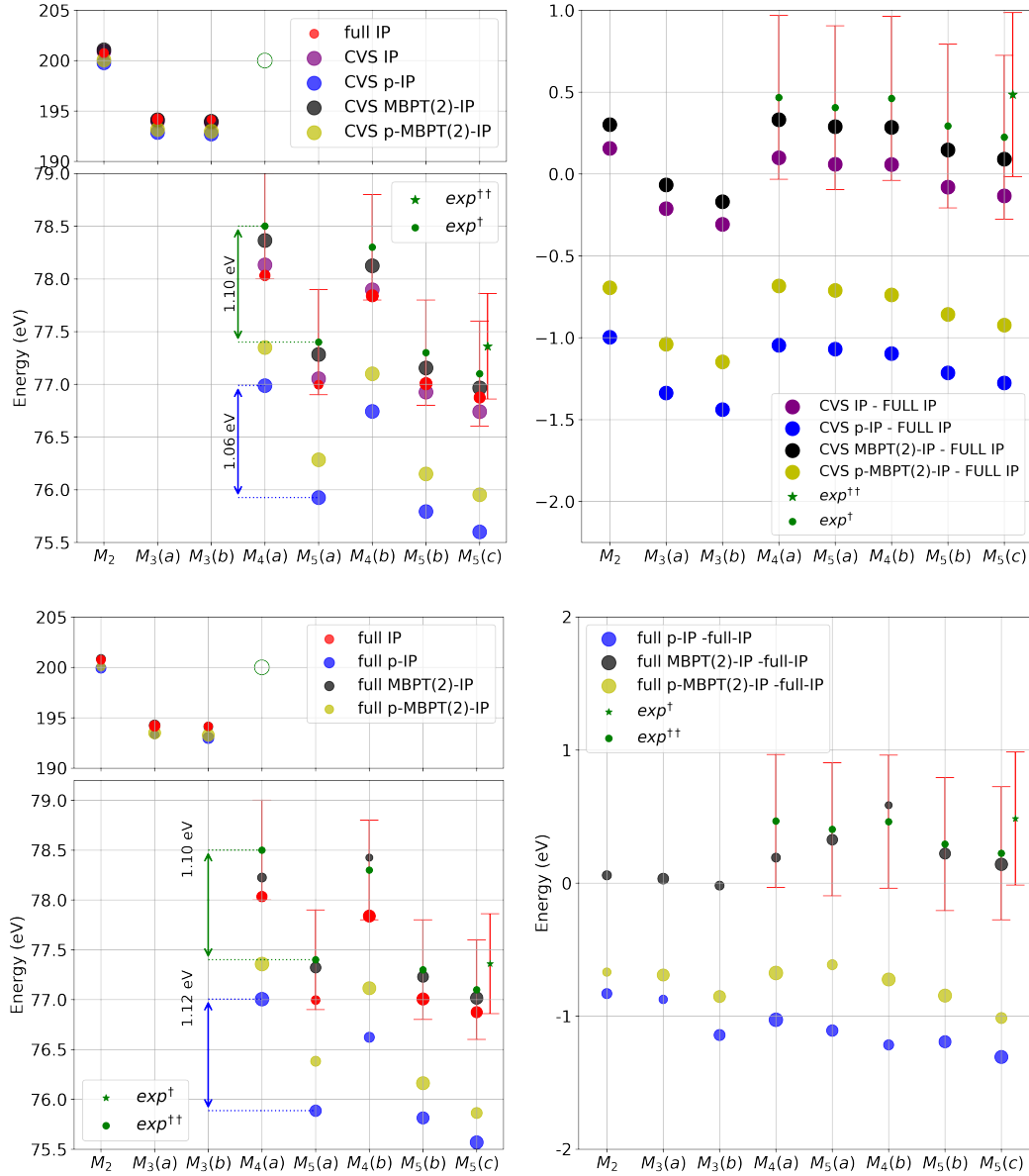


TABLE II: Energy 'E' (in eV) and the  $\%SI = 100 \left( (r_i)_k \right)^2$  of the selected solution for HBr.  $\Delta_f$  is the difference w.r.t. full-IP and  $\Delta_{IP}$  is the difference IP<sub>App</sub>-IP - 'mean' and 'std' for the M edge, respectively : the mean and the standard deviation of the difference in energie . For experimental data precision of  $\pm 0.5$  eV.

T	full-IP		IP		P-IP			PT(2)			P-PT(2)			full-P-IP		full-PT(2)		full-P-PT(2)		exp <sup>†</sup>
	E <sub>f</sub>	%SI	$\Delta_f$	%SI	$\Delta_f$	$\Delta_{IP}$	%SI	$\Delta_f$	$\Delta_{IP}$	%SI	$\Delta_f$	$\Delta_{IP}$	%SI	$\Delta_f$	%SI	$\Delta_f$	%SI	$\Delta_f$	%SI	
<i>M</i> <sub>2</sub>	200.765	36	0.156	90	-0.997	-1.153	89	0.301	0.145	90	-0.695	-0.851	90	-0.830	48	0.058	40	-0.668	33	
<i>M</i> <sub>3</sub> ( <i>a</i> )	194.210	50	-0.213	90	-1.337	-1.125	89	-0.067	0.145	91	-1.039	-0.827	90	-0.873	34	0.034	55	-0.691	68	
<i>M</i> <sub>3</sub> ( <i>b</i> )	194.151	33	-0.307	90	-1.439	-1.131	89	-0.169	0.138	91	-1.147	-0.839	90	-1.141	58	-0.019	39	-0.851	67	
M edge 3 <i>p</i>																				
mean			-0.121		-1.258	-1.136		0.022	0.143		-0.960	-0.839		-0.948		0.025		-0.737		
std			0.200		0.189	0.012		0.202	0.003		0.193	0.010		0.138		0.032		0.082		
<i>M</i> <sub>4</sub> ( <i>a</i> )	78.033	50	0.099	90	-1.046	-1.145	89	0.331	0.232	91	-0.684	-0.783	89	-1.027	86	0.191	38	-0.675	87	78.5 <sup>?</sup>
<i>M</i> <sub>5</sub> ( <i>a</i> )	76.995	35	0.059	90	-1.070	-1.129	89	0.289	0.230	91	-0.711	-0.770	89	-1.108	61	0.327	53	-0.613	47	77.4 <sup>?</sup>
<i>M</i> <sub>4</sub> ( <i>b</i> )	77.839	67	0.058	90	-1.097	-1.155	89	0.285	0.227	91	-0.739	-0.796	89	-1.215	48	0.587	24	-0.724	80	78.0 <sup>?</sup>
<i>M</i> <sub>5</sub> ( <i>b</i> )	77.008	68	-0.081	90	-1.214	-1.134	89	0.147	0.228	91	-0.858	-0.777	89	-1.193	69	0.223	57	-0.845	80	77.3 <sup>?</sup>
<i>M</i> <sub>5</sub> ( <i>c</i> )	76.876	58	-0.134	90	-1.277	-1.142	89	0.090	0.224	91	-0.923	-0.789	89	-1.306	80	0.141	73	-1.013	57	77.1 <sup>?</sup> ; 77.36 <sup>?</sup>
M edge 3 <i>d</i>																				
mean			<1e-4		-1.141	-1.141		0.228	0.228		-0.783	-0.783		-1.170		0.294		-0.774		
std			0.091		0.089	0.009		0.093	0.003		0.092	0.009		0.095		0.159		0.142		

FIG. 2: Energies (in eV) for HBr - Comparison between CVS  $IP_{AppS}$  and full-IP for the M edge for the 2 upper graph, for the two second it is the comparison between  $IP_{AppS}$  full diagonalized and full-IP, all values in eV. The points have a size proportional to  $\%SI = 100 \left( (r_i)_k \right)^2$ , to compare, in the first block, the green circle corresponds to a  $\%SI$  of 100%. Experimental data  $^{†?}$ ;  $^{††?}$  are given with error bars.



### C. Valence Ionization Potential for $XO^-$ ( $X \in [Cl; Br; I; At; Ts]$ )

TABLE III: Four first IP for  $XO^-$  ( $X \in [Cl; Br; I; At; Ts]$ ) - Energy 'E' (in eV) and the  $\%SI = 100 \left( \frac{(r_i)_k}{r_k} \right)^2$  of the selected solution.  $\Delta_{IP}$  is the difference  $IP_{App} - IP$  and  $\Delta_{exp}$  is the difference w.r.t. experimental.

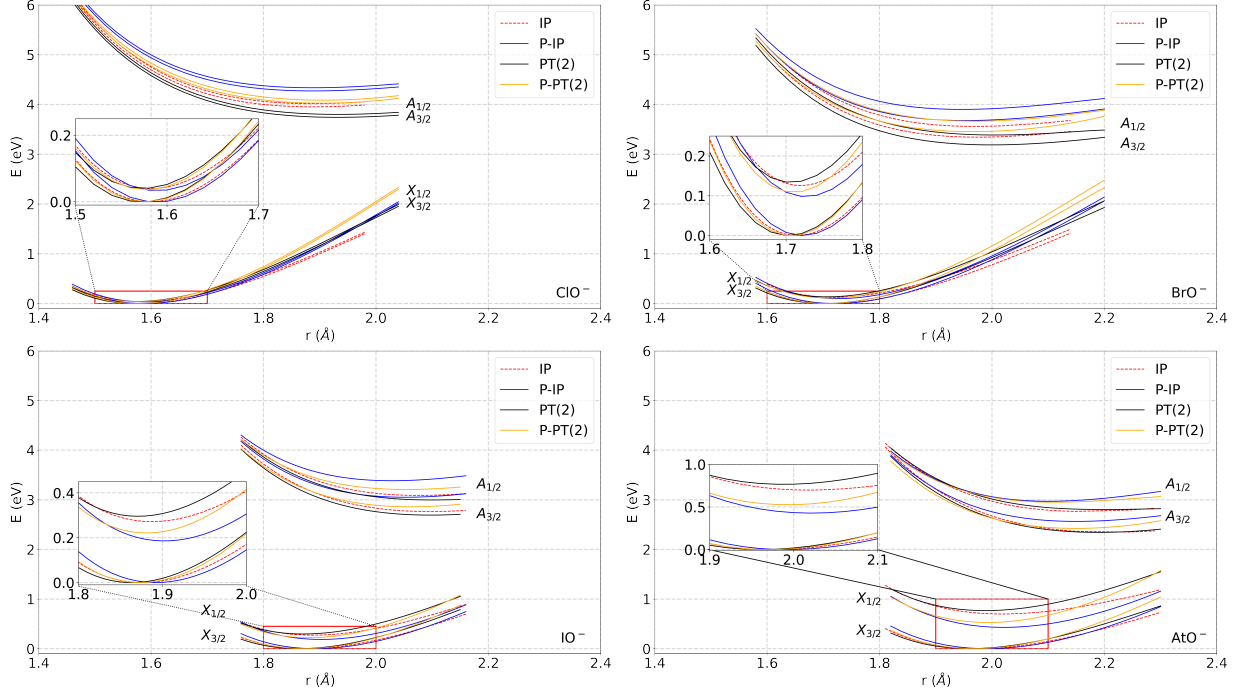
T	IP		P-IP		PT(2)		P-PT(2)		
	E	%SI	%SI	$\Delta_{IP}$	%SI	$\Delta_{IP}$	%SI	$\Delta_{IP}$	
ClO <sup>-</sup>	X <sub>3/2</sub>	2.040	91	86	-0.524	92	0.062	88	-0.359
	X <sub>1/2</sub>	2.083	91	86	-0.530	92	0.063	88	-0.363
	A <sub>3/2</sub>	6.855	89	85	-0.292	90	-0.057	87	-0.295
	A <sub>1/2</sub>	6.914	87	82	-0.291	88	-0.058	85	-0.294
exp <sup>?</sup>	$\Delta_{exp}$		$\Delta_{exp}$		$\Delta_{exp}$		$\Delta_{exp}$		
	X <sub>1/2</sub>	2.276	-0.1933		-0.7231		-0.1299		-0.5563
BrO <sup>-</sup>	X <sub>3/2</sub>	2.149	88	82	-0.549	90	0.105	85	-0.330
	X <sub>1/2</sub>	2.280	88	82	-0.577	90	0.112	85	-0.348
	A <sub>3/2</sub>	6.126	87	81	-0.329	88	-0.007	83	-0.286
	A <sub>1/2</sub>	6.314	64	53	-0.327	68	-0.007	61	-0.276
exp <sup>?</sup>	$\Delta_{exp}$		$\Delta_{exp}$		$\Delta_{exp}$		$\Delta_{exp}$		
	X <sub>1/2</sub>	2.353	-0.0732		-0.6502		0.0387		-0.4213
IO <sup>-</sup>	X <sub>3/2</sub>	2.238	86	76	-0.547	89	0.114	81	-0.300
	X <sub>1/2</sub>	2.518	85	75	-0.630	87	0.137	79	-0.352
	A <sub>3/2</sub>	5.455	84	74	-0.399	86	0.038	78	-0.313
	A <sub>1/2</sub>	5.705	49	55	-0.402	43	0.053	47	-0.274
exp <sup>?</sup>	$\Delta_{exp}$		$\Delta_{exp}$		$\Delta_{exp}$		$\Delta_{exp}$		
	X <sub>1/2</sub>	2.378	0.1398		-0.4905		0.2766		-0.2121
AtO <sup>-</sup>	X <sub>3/2</sub>	1.888	84	70	-0.604	87	0.255	76	-0.220
	X <sub>1/2</sub>	2.620	71	59	-0.874	72	0.310	62	-0.406
	A <sub>3/2</sub>	4.672	81	67	-0.552	83	0.208	72	-0.294
	A <sub>1/2</sub>	4.943	68	61	-0.546	68	0.295	62	-0.169
TsO <sup>-</sup>	X <sub>3/2</sub>	1.292	83	57	-0.741	87	0.258	68	-0.259
	X <sub>1/2</sub>	2.501	88	81	-1.379	89	0.397	84	-0.713
	A <sub>3/2</sub>	3.525	78	52	-0.764	82	0.263	63	-0.465
	A <sub>1/2</sub>	3.582	90	84	-0.759	91	0.414	86	-0.232

### D. Potential Energy Curves - $XO^-$ with $X \in [Cl; Br; I; At]$

With the curves, we studied position of the minima, the difference w.r.t. EOM-IP and the energies of transition between levels.

## 1. Graphics

FIG. 3: *Potential Energy Curves* for all the compounds with  $X \in [\text{Cl}; \text{Br}; \text{I}; \text{At}]$  and all approximated methods  $\text{IP}_{\text{App}}$ . The energy :  $E$  in eV and the distance  $X\text{-O}$  :  $r$  in  $\text{\AA}$ . The overlay graphic is the zoom of the red rectangle.



## 2. Tables : Position of minima

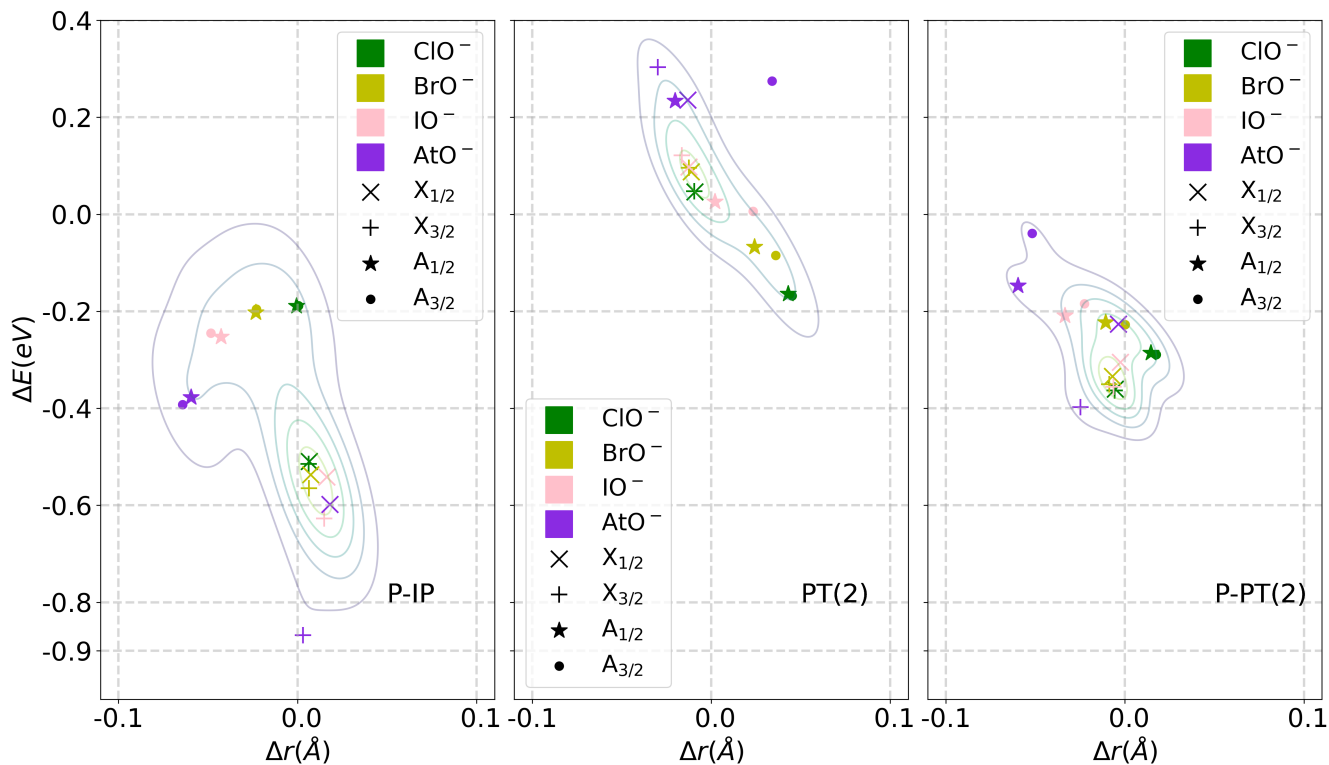
TABLE IV: Minimum of the *Potential Energy Curve* for  $\text{XO}^-$  with  $X \in [\text{Cl}; \text{Br}; \text{I}; \text{At}]$ .  $E_{MO}$  is the absolute energy (in eV), and  $r$  the distance  $X\text{-O}$  of the minimum (in  $\text{\AA}$ ).  $\Delta_r$  is difference between minimum length, and  $\Delta_E$  is difference between minimum energy.

T		IP		P-IP		PT(2)		P-PT(2)	
		$r$	$E_{MO}$	$\Delta_r$	$\Delta_E$	$\Delta_r$	$\Delta_E$	$\Delta_r$	$\Delta_E$
$\text{ClO}^-$	$X_{3/2}$	1.5818	-10.9061	0.0065	-0.5095	-0.0092	0.0465	-0.0054	-0.3601
	$X_{1/2}$	1.5828	-10.8665	0.0063	-0.5148	-0.0094	0.0477	-0.0057	-0.3634
	$A_{3/2}$	1.8889	-6.9541	-0.0006	-0.1888	0.0429	-0.1638	0.0145	-0.2859
	$A_{1/2}$	1.8875	-6.8909	0.0004	-0.1883	0.0451	-0.1678	0.0175	-0.2893
$\text{BrO}^-$	$X_{3/2}$	1.7141	-7.2208	0.0073	-0.5370	-0.0112	0.0878	-0.0070	-0.3341
	$X_{1/2}$	1.7192	-7.0952	0.0064	-0.5649	-0.0125	0.0958	-0.0088	-0.3505
	$A_{3/2}$	1.9751	-3.8787	-0.0234	-0.2027	0.0242	-0.0673	-0.0108	-0.2226
	$A_{1/2}$	1.9692	-3.6622	-0.0229	-0.1957	0.0360	-0.0848	0.0001	-0.2277
$\text{IO}^-$	$X_{3/2}$	1.8758	-26.7779	0.0164	-0.5414	-0.0124	0.0974	-0.0026	-0.3049
	$X_{1/2}$	1.8874	-26.5063	0.0149	-0.6274	-0.0165	0.1214	-0.0063	-0.3554
	$A_{3/2}$	2.0950	-24.0159	-0.0427	-0.2527	0.0020	0.0263	-0.0334	-0.2087
	$A_{1/2}$	2.0767	-23.6909	-0.0484	-0.2448	0.0234	0.0064	-0.0227	-0.1845
$\text{AtO}^-$	$X_{3/2}$	1.9734	-20.3352	0.0181	-0.5979	-0.0131	0.2357	-0.0037	-0.2263
	$X_{1/2}$	2.0180	-19.6367	0.0031	-0.8677	-0.0298	0.3031	-0.0248	-0.3974
	$A_{3/2}$	2.2090	-17.9910	-0.0594	-0.3774	-0.0201	0.2337	-0.0597	-0.1468
	$A_{1/2}$	2.1645	-17.5705	-0.0642	-0.3925	0.0339	0.2746	-0.0517	-0.0394

### 3. Graphic representation of positions and energies minima errors in PES for $XO^-$

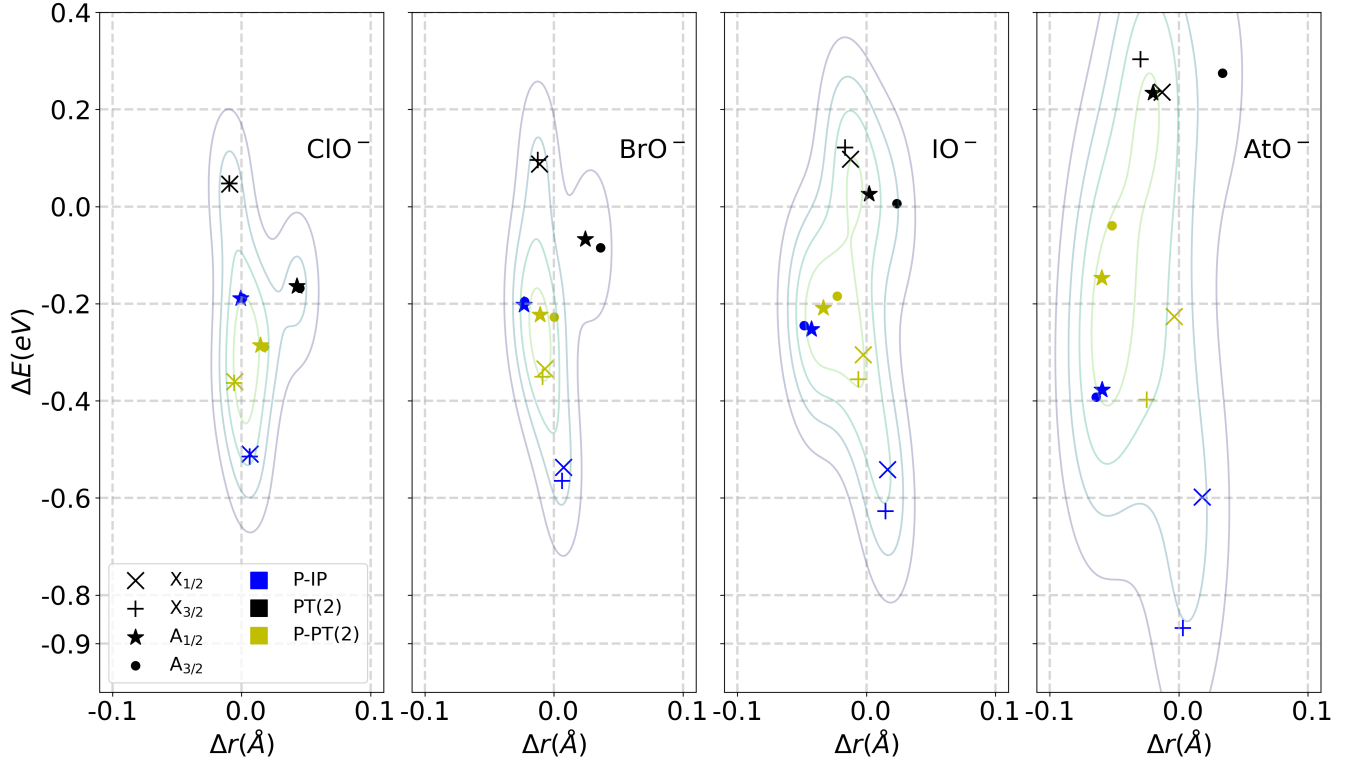
As reminder of the paper the figure (fig.4) is again reported here. Symbols represent the error in energy and in position of the minimum of the Potential Energy Curves ( $\Delta E$  (in eV) w.r.t.  $\Delta r$  ( $\text{\AA}$ )).

FIG. 4: Difference in the PES minimums positions and energies -  $\Delta E$  (in eV) w.r.t.  $\Delta r$  ( $\text{\AA}$ ) for the 3  $IP_{App}$  and the 4 compounds. For reasons of readability : colors for compounds and symbols for states. The 4 different isodensities represented were calculated by a Gaussian kde algorithm<sup>2</sup>, resp. in  $[-0.1; 0.1]$  ( $\text{\AA}$ ),  $[-1.0; 0.4]$  (eV) limits for  $\Delta r$  and  $\Delta E$ .



For the second graph (fig.5), the information is obviously identical, but on reading we can easily see the increase in the error for P-IP and the solution  $X_{1/2}$  as we move down the halogen column. We notice that the errors for  $A_{3/2}$  and  $A_{1/2}$  are independent of the magnitude of the spin-orbit coupling.

FIG. 5: Difference in the *PES* minimums position and energies  $-\Delta E$  (in eV) w.r.t.  $\Delta r$  ( $\text{\AA}$ ) for the 3  $\text{IP}_{\text{App}}$  and the 4 compounds. For reasons of readability : colors for  $\text{IP}_{\text{App}}$ s and symbols for states. The 4 different isodensities represented were calculated by a Gaussian kde algorithm<sup>2</sup>, resp. in  $[-0.1; 0.1]$  ( $\text{\AA}$ ),  $[-1.0; 0.4]$  (eV) limits for  $\Delta r$  and  $\Delta E$ .



#### 4. Energies of transitions

TABLE V: Transition energies  $\Delta_E$  (in eV) for  $\text{XO}^-$  with  $\text{X} \in [\text{Cl}; \text{Br}; \text{I}; \text{At}]$ . and difference with  $\Delta_{\text{IP}}$ .

$\Delta_T$	$\Delta_E$				$\Delta_E - \Delta_{\text{IP}}$			
	$\Delta_{\text{IP}}$	$\Delta_{\text{P-IP}}$	$\Delta_{\text{PT(2)}}$	$\Delta_{\text{P-PT(2)}}$	$\Delta_{\text{P-IP}} - \Delta_{\text{IP}}$	$\Delta_{\text{PT(2)}} - \Delta_{\text{IP}}$	$\Delta_{\text{P-PT(2)}} - \Delta_{\text{IP}}$	
$\text{ClO}^-$	$X_{3/2}-X_{3/2}$	0.0000	0.0000	0.0000	0.0000	0.0000	0.0000	
	$X_{1/2}-X_{3/2}$	0.0396	0.0343	0.0408	0.0363	-0.0054	-0.0034	
	$A_{3/2}-X_{3/2}$	3.9520	4.2727	3.7418	4.0262	0.3207	-0.2103	0.0741
	$A_{1/2}-X_{3/2}$	4.0153	4.3364	3.8009	4.0860	0.3212	-0.2144	0.0708
$\text{BrO}^-$	$X_{3/2}-X_{3/2}$	0.0000	0.0000	0.0000	0.0000	0.0000	0.0000	
	$X_{1/2}-X_{3/2}$	0.1256	0.0978	0.1336	0.1092	-0.0279	0.0080	-0.0164
	$A_{3/2}-X_{3/2}$	3.3421	3.6764	3.1871	3.4536	0.3344	-0.1550	0.1115
	$A_{1/2}-X_{3/2}$	3.5586	3.8999	3.3860	3.6650	0.3414	-0.1726	0.1065
$\text{IO}^-$	$X_{3/2}-X_{3/2}$	0.0000	0.0000	0.0000	0.0000	0.0000	0.0000	
	$X_{1/2}-X_{3/2}$	0.2717	0.1856	0.2956	0.2211	-0.0860	0.0240	-0.0505
	$A_{3/2}-X_{3/2}$	2.7620	3.0507	2.6909	2.8583	0.2887	-0.0711	0.0962
	$A_{1/2}-X_{3/2}$	3.0870	3.3835	2.9960	3.2074	0.2966	-0.0910	0.1204
$\text{AtO}^-$	$X_{3/2}-X_{3/2}$	0.0000	0.0000	0.0000	0.0000	0.0000	0.0000	
	$X_{1/2}-X_{3/2}$	0.6985	0.4287	0.7659	0.5274	-0.2698	0.0674	-0.1711
	$A_{3/2}-X_{3/2}$	2.3442	2.5647	2.3422	2.4237	0.2205	-0.0020	0.0795
	$A_{1/2}-X_{3/2}$	2.7647	2.9701	2.8036	2.9516	0.2055	0.0389	0.1869

It is therefore possible to use the  $\text{IP}_{\text{App}}$  methods to determine the transition energies between the different levels. We can compare these transition energies with experimental values (tab. VI). This table shows the transition energy  $\Delta_T = X_{1/2} - X_{3/2}$  for the different approximations. Reading this table, the conclusions remain the same. We can also notice that the method

P-MBPT(2)-IP remains correct until iodine with an error of  $\sim 0.04$  eV.

TABLE VI: Transition energies  $\Delta T_{\text{method}}$  between  $X_{1/2}-X_{3/2}$  for  $\text{ClO}^-$ ,  $\text{BrO}^-$  and  $\text{IO}^-$ , comparison with experimental data (in eV).

$\Delta T: X_{1/2}-X_{3/2}$	exp <sup>2</sup>	$\Delta T_{\text{IP}}$	$\Delta T_{\text{P-IP}}$	$\Delta T_{\text{PT(2)}}$	$\Delta T_{\text{P-PT(2)}}$
$\text{ClO}^-$	0.0397	0.0396	0.0343	0.0408	0.0363
$\text{BrO}^-$	0.1270	0.1256	0.0977	0.1336	0.1092
$\text{IO}^-$	0.2593	0.2717	0.1856	0.2956	0.2211

### E. $\text{I}_3^-$

Paper presents data for  ${}^2\text{DCG}^{\text{M}}$ , i.e. with Gaunt, here are tables for  $\text{I}_3^-$  values for IP, EE, and EA with  ${}^2\text{DC}^{\text{M}}$ .

TABLE VII: Ionization potential (in eV) for  $\text{I}_3^-$ ,  ${}^2\text{DC}^{\text{M}}$  hamiltonian,  $\%SI = 100 \left( \frac{(r_i)_k}{r_i} \right)^2$  in [89%; 93%] in all case

T	$\Delta_{\text{IP}}$				$\Delta_{\text{exp}}$				
	IP	P-IP	PT(2)	P-PT(2)	exp <sup>2</sup>	IP	P-IP	PT(2)	P-PT(2)
$\text{IP}_1^{1/2g}$	4.467	-0.053	0.104	0.059	4.53	-0.063	-0.116	0.041	-0.004
$\text{IP}_2^{3/2g}$	4.995	-0.139	0.010	-0.096	4.93	0.065	-0.074	0.075	-0.032
$\text{IP}_3^{1/2u}$	4.915	-0.098	0.042	-0.034	4.87	0.045	-0.053	0.088	0.011
$\text{IP}_4^{3/2u}$	4.282	-0.100	0.041	-0.037	4.25	0.032	-0.067	0.073	-0.004
mean		-0.097	0.049	-0.027		0.020	-0.078	0.069	-0.007
std		0.030	0.034	0.056		0.049	0.023	0.017	0.015

TABLE VIII: Excitation Energies (in eV) for  $\text{I}_3^-$ ,  ${}^2\text{DC}^{\text{M}}$  hamiltonian,  $\%SE = 100 \left( \frac{(r_i)_k}{r_i} \right)^2$ . In bold characters the reversed levels. Experimental data for  $(0_u^+)$ : 3.43 4.25<sup>2</sup> 3.45 4.28<sup>2</sup>.

T	EE		P-EE		PT(2)		P-PT(2)		$\text{CASPT2}^2$	
	EE	%SE	%SE	$\Delta$	%SE	$\Delta$	%SE	$\Delta$	E	$\Delta$
$2_g^-$	2.2422	43	45	0.2627	43	0.0036	45	0.2655	2.24	-0.0022
$1_g^-$	2.3703	23	24	0.2527	23	<b>0.1139</b>	24	<b>0.3683</b>	2.32	-0.0503
$0_u^-$	2.3749	41	43	<b>0.2664</b>	41	<b>0.0037</b>	43	<b>0.2687</b>	2.47	0.0951
$1_u^-$	2.3770	46	48	<b>0.2537</b>	46	0.1142	48	0.3696	2.47	0.0930
$0_g^-$	2.8384	22	22	0.2712	22	0.0044	22	0.2751	2.76	-0.0784
$0_u^+$	2.8936	22	22	0.2724	22	0.0034	22	0.2744	2.82	-0.0736
$1_g^+$	3.0665	42	43	0.2805	42	0.0062	43	0.2846	2.85	-0.2165
$2_u^+$	3.3242	48	50	0.2553	48	-0.0135	50	0.2429	3.10	-0.2242
$1_u^+$	3.4090	48	50	0.2609	48	-0.0136	50	0.2470	3.11	-0.2990
$0_u^+$	3.6630	18	20	0.2434	18	-0.0148	19	0.2248	3.52	-0.1430
$2_g^+$	4.0797	24	24	0.2692	24	-0.0085	24	0.2627	3.98	-0.0997
$0_u^-$	4.0888	42	43	0.2871	42	-0.0101	43	0.2752	3.79	-0.2988
$1_g^-$	4.1836	47	49	0.2764	47	-0.0092	49	0.2668	4.06	-0.1236
$1_u^-$	4.2087	40	41	0.3010	40	-0.0044	41	0.2934	3.80	-0.4087
$0_u^+$	4.4894	16	17	0.2433	16	0.0007	17	0.2403	4.51	0.0206
$0_g^-$	4.6890	20	21	0.2987	20	-0.0105	21	0.2867	4.51	-0.1790
$0_u^+$	4.7004	20	21	0.2996	20	-0.0095	21	0.2885	4.53	-0.1704
$1_g^+$	4.9025	40	36	<b>0.3025</b>	40	0.0073	24	<b>0.3325</b>	4.60	-0.3025
mean				0.2721		0.0091		0.2815		-0.1367
std				0.0189		0.0378		0.0386		0.1368

TABLE IX: Electronic Affinities (in eV) for  $I_3^-$ ,  ${}^2DC^M$  hamiltonian,  $\%SA = 100((r^a)_k)^2$ .

T	EA		P-EA		PT(2)		P-PT(2)	
	E	%SA	%SA	$\Delta_{EA}$	%SA	$\Delta_{EA}$	%SA	$\Delta_{EA}$
EA $_1^{1/2u}$	2.5069	76	76	-0.0229	76	-0.0144	74	-0.0538
EA $_2^{1/2u}$	3.6445	77	77	0.0076	76	0.0038	75	0.0092
EA $_3^{1/2g}$	3.8780	94	94	0.0121	94	0.0179	95	0.0322
EA $_4^{1/2u}$	4.3892	96	96	0.0096	96	0.0003	96	0.0087
mean				0.0016		0.0019		-0.0009
std				0.0143		0.0115		0.0320

F.  $CH_2I_2 - CH_2IBr$ 

Paper presents data for  ${}^2DCG^M$ , i.e. with Gaunt, here are tables for  $CH_2I_2$  and  $CH_2IBr$  EA with  ${}^2DC^M$ .

TABLE X: Electronic Affinities (in eV) for  $CH_2I_2$ ,  ${}^2DC^M$  hamiltonian,  $\%SA = 100((r^a)_k)^2$ .

T	EA		P-EA		PT(2)		P-PT(2)	
	E	%SA	%SA	$\Delta_{EA}$	%SA	$\Delta_{EA}$	%SA	$\Delta_{EA}$
EA $_1$	-0.3277	48	50	-0.0617	48	-0.0575	49	-0.0971
EA $_2$	0.4105	57	60	0.0045	58	-0.0082	60	0.0003
EA $_3$	0.7549	83	80	-0.0175	82	-0.0095	80	-0.0167
EA $_4$	0.8565	98	98	0.0066	98	-0.0086	98	0.0007
EA $_5$	1.4908	87	86	0.0103	86	-0.0022	85	0.0116
EA $_6$	1.6984	67	61	-0.0074	65	-0.0125	61	-0.0102
mean				-0.0109		-0.0164		-0.0186
std				0.0246		0.0186		0.0362
exp $^?$		$\Delta_{exp}$		$\Delta_{exp}$		$\Delta_{exp}$		$\Delta_{exp}$
ET $_2$	0.68	-0.2695		-0.2649		-0.2777		-0.2692
DA $_2$	0.46	-0.0495		-0.0449		-0.0577		-0.0492

TABLE XI: Electronic Affinities (in eV) for  $CH_2IBr$ ,  ${}^2DC^M$  hamiltonian,  $\%SA = 100((r^a)_k)^2$ .

T	EA		P-EA		PT(2)		P-PT(2)	
	E	%SA	%SA	$\Delta_{EA}$	%SA	$\Delta_{EA}$	%SA	$\Delta_{EA}$
EA $_1$	-0.0255	52	53	-0.0417	52	-0.0589	53	-0.0823
EA $_2$	0.4487	66	70	0.0037	67	-0.0096	70	-0.0014
EA $_3$	0.8554	97	97	0.0072	97	-0.0086	97	0.0009
EA $_4$	0.9897	87	85	-0.0025	86	-0.0096	85	-0.0048
EA $_5$	1.6154	70	69	0.0080	68	-0.0061	67	0.0063
EA $_6$	1.9166	51	49	0.0000	55	-0.0121	48	-0.0047
mean				-0.0042		-0.0175		-0.0143
std				0.0171		0.0186		0.0306

$CH_2I_2$  EE with  ${}^2DC^M$ .

TABLE XII: Excitation Energies (in eV) for  $\text{CH}_2\text{I}_2$ ,  ${}^2\text{DC}^{\text{M}}$  hamiltonian,  $\%SE = 100 \left( \left( r_i^a \right)_k \right)^2$ .

T	EE		P-EE		PT(2)		P-PT(2)	
	EE	%SE	%SE	$\Delta$	%SE	$\Delta$	%SE	$\Delta$
a	3.6032	20	21	0.2873	20	-0.0689	21	0.2274
b	3.6168	20	20	0.2879	20	-0.0670	20	0.2300
a	3.6280	20	21	0.2885	20	-0.0652	21	0.2326
b	3.8444	16	17	0.2955	15	-0.0729	16	0.2302
a	3.8684	19	19	0.2946	19	-0.0683	19	0.2339
b	3.9421	13	13	0.3062	13	-0.0773	13	0.2359
a	3.9936	16	17	0.3022	16	-0.0760	17	0.2336
b	4.0597	16	16	0.3084	16	-0.0714	16	0.2439
b	4.2220	18	19	0.2970	18	-0.0604	19	0.2448
a	4.3222	15	16	0.3011	15	-0.0726	16	0.2365
b	4.3522	15	15	0.3056	15	-0.0597	15	0.2538
a	4.4937	14	15	0.3072	15	-0.0691	16	0.2449
b	4.6384	15	15	0.3241	15	-0.0737	15	0.2584
a	4.6829	16	17	0.3489	17	-0.0647	18	0.2922
b	4.7499	15	14	0.3388	15	-0.0718	15	0.2752
a	4.9106	14	15	0.3512	15	-0.0617	15	0.2962
mean				0.3090		-0.0688		0.2481
std				0.0201		0.0052		0.0212